

Analytical Investigation of the Dynamics
of Tethered Constellations in Earth Orbit (Phase II)

Contract NAS8-36606

Quarterly Report #5

For the period 22 March 1986 through 21 June 1986

Principal Investigator

Dr. Enrico C. Lorenzini

July 1986

Prepared for
National Aeronautics and Space Administration
Marshall Space Flight Center, Alabama 35812

Smithsonian Institution
Astrophysical Observatory
Cambridge, Massachusetts 02138

The Smithsonian Astrophysical Observatory
is a member of the
Harvard-Smithsonian Center for Astrophysics

(NASA-CR-178901). ANALYTICAL INVESTIGATION
OF THE DYNAMICS OF TETHERED CONSTELLATIONS
IN EARTH ORBIT, PHASE 2 (Smithsonian
Astrophysical Observatory) 59 p CSCL 22A

N86-32513

Unclas
G3/18 44662

Analytical Investigation of the Dynamics
of Tethered Constellations in Earth Orbit (Phase II)

Contract NAS8-36606

Quarterly Report #5

For the period 22 March 1986 through 21 June 1986

Principal Investigator
Dr. Enrico C. Lorenzini

Co-Investigators
Mr. David A. Arnold
Mr. Mario Cosmo
Dr. Mario D. Grossi

July 1986

Prepared for
National Aeronautics and Space Administration
Marshall Space Flight Center, Alabama 35812

Smithsonian Institution
Astrophysical Observatory
Cambridge, Massachusetts 02138

The Smithsonian Astrophysical Observatory
is a member of the
Harvard-Smithsonian Center for Astrophysics

CONTENTS

	Page
Abstract	3
Figure Captions	4
SECTION 1.0 INTRODUCTION	5
2.0 TECHNICAL ACTIVITY DURING REPORTING PERIOD AND PROGRAM STATUS	5
2.1 3-Dimensional Model Of The 4-Mass Tethered System	5
2.2 Software Implementation Of The 3-Dimensional Model And New Integration Subroutine	12
2.3 Simulation Runs Of The Station Keeping Phase Of The 4- Mass Tethered System With/Without Longitudinal Dampers	14
2.4 Damping Algorithms For In-Plane Librational And Lateral Oscillatory Modes	32
2.5 Station-Keeping Simulation Runs With/Without Librational And Lateral Damping Algorithms	34
2.6 Concluding Remarks	57
3.0 PROBLEMS ENCOUNTERED DURING REPORTING PERIOD	58
4.0 ACTIVITY PLANNED FOR THE NEXT REPORTING PERIOD	58

Abstract

This quarterly report deals with the analytical model and software implementation of n-mass, three dimensional tethered systems. The newly developed computer code is then used for simulating the 3-dimensional dynamics of a 4-mass tethered system. The 4-mass tethered system is designed in order to provide a micro-g environment on board the Space Station while variable-g experiments are performed on a laboratory moving along the upward tether segment. Extensive simulation runs illustrate both the undamped, free response and the damped dynamics response of the system. Passive longitudinal dampers and subsequently active damping algorithms, effective against the in-plane dynamics, are added to the system. Their separate effects upon the various vibrational modes are clearly shown by relevant simulation runs.

PRECEDING PAGE BLANK NOT FILMED

1,2

Figure Captions

- Figure 2.1.1 Geometry for the n-mass, 3-dimensional tethered system.
- Figure 2.1.2 Schematic of the relationships between generalized coordinates and Cartesian coordinates.
- Figure 2.3.1 Schematic of the 4-mass tethered system for micro-g/variable-g applications.
- Figure 2.3.2a-v Three-dimensional, free dynamic response of the 4-mass tethered system without dampers for a 7200 sec station-keeping phase. Figures 2.3.2t and u show the side-view and front-view of the system at 20 sec intervals for 3600 sec. Figure 2.3.2v is the equal scale, side-view at 20 sec intervals for 1000 sec (simulation run no. 1).
- Figure 2.3.3a-m Three-dimensional, free dynamic response of the 4-mass tethered system with 3 longitudinal dampers in series with the associated tether segments. Same initial conditions of simulation run no. 1. Station-keeping phase of 7200 sec (simulation run no. 2).
- Figure 2.5.1a-za Three-dimensional, free dynamic response of the 4-mass tethered system with 3 longitudinal dampers for initial condition 90° out-of-phase with respect to simulation runs no. 1 and 2. Station-keeping phase of 7200 sec. Figures 2.5.1z and za show the side-view and front-view of the system at 40 sec intervals for 7200 sec (simulation run no. 3).
- Figure 2.5.2a-za Three-dimensional, free dynamic response of the 4-mass tethered system with longitudinal dampers and with in-plane librational/lateral damping algorithms. Same initial conditions of simulation run no. 3. Station-keeping phase of 10,000 sec. Figures 2.5.2z and az show the side-view and the front-view of the system at 40 sec intervals for 7200 sec only. (Simulation run no. 4).

1.0 INTRODUCTION

This is the fifth quarterly report submitted by SAO under contract NAS8-36606, "Analytical Investigation of the Dynamics of Tethered Constellations in Earth Orbit (Phase II)," Dr. Enrico C. Lorenzini, PI. This report covers the period from 22 March 1986 through 21 June 1986.

2.0 TECHNICAL ACTIVITY DURING REPORTING PERIOD AND PROGRAM STATUS

2.1 3-Dimensional Model Of The 4-Mass Tethered System

The 2-dimensional equations of motion (Cartesian coordinates) derived for the n-mass system in Section 2.3 of Quarterly Report No. 3 have been extended to the third dimension.

The derivation of the 3-dimensional equations of motion follows the line shown in Section 2.3 of Quarterly Report No. 3 with the addition of the out-of-plane coordinate y . With reference to Figure 2.1.1 the radius vector $\vec{\rho}_i$ from the origin of the orbiting reference frame to the i^{th} -mass is given by:

$$\vec{\rho}_i = x_i \vec{i} + y_i \vec{j} + z_i \vec{k} \quad (2.1.1)$$

The inertial acceleration of the i^{th} -mass is given by:

$$\ddot{\vec{r}}_{Ii} = \ddot{\vec{\rho}}_i + 2\vec{\Omega} \times \dot{\vec{\rho}}_i + \vec{\Omega} (\vec{\Omega} \cdot \vec{r}_i) - \vec{r}_i |\vec{\Omega}|^2 \quad (2.1.2)$$

where:

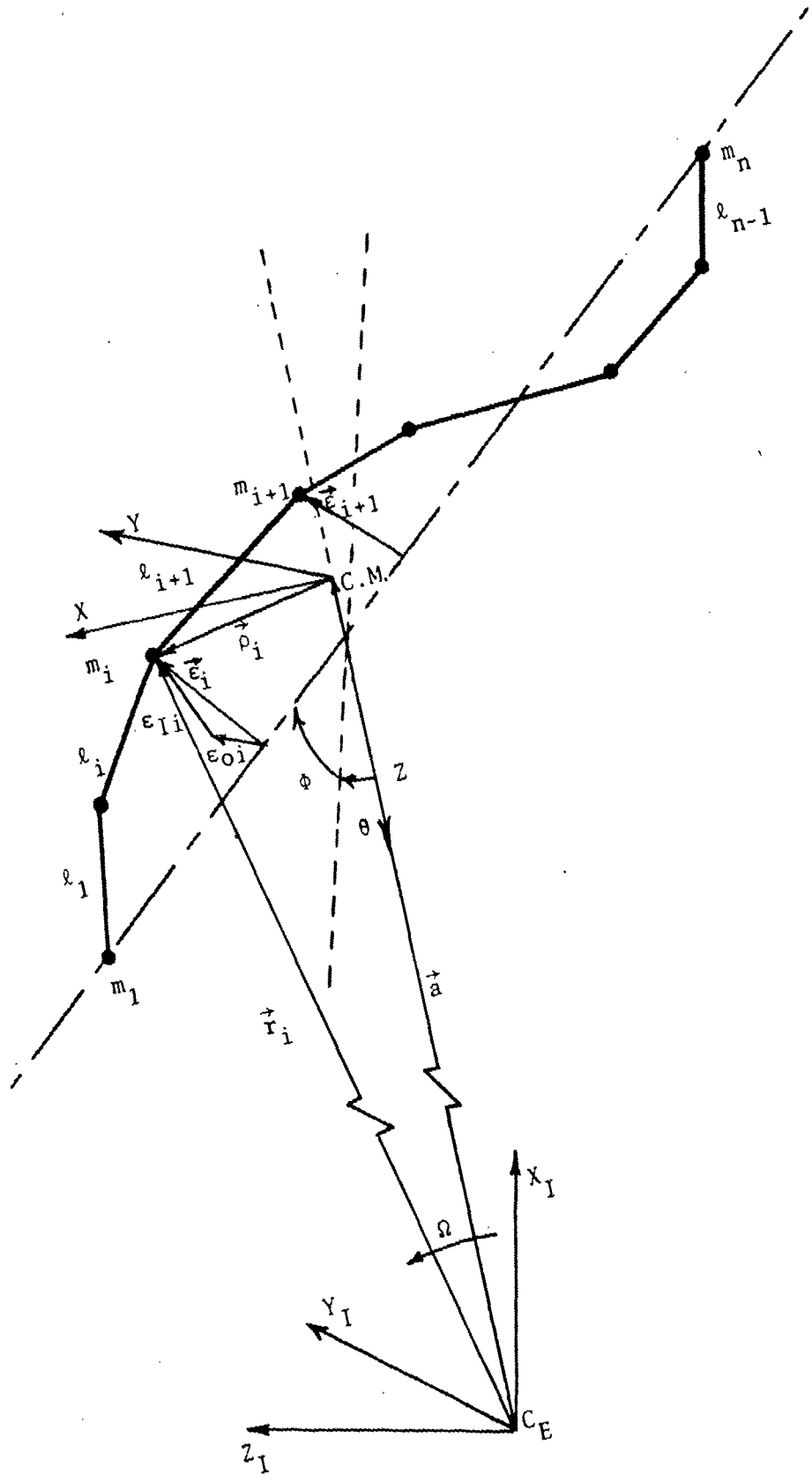


Figure 2.1.1

$$\vec{r}_i = \vec{a} + \vec{\rho}_i \quad (2.1.3)$$

After substitution of equations (2.1.2) and (2.1.3) into equation (2.1.1) we finally get:

$$\ddot{\vec{r}}_{I1} = [\ddot{x}_i - 2\Omega \dot{z}_i - \Omega^2 x_i] \vec{i} + [\ddot{y}_i] \vec{j} + [\ddot{z}_i + 2\Omega \dot{x}_i - \Omega^2(z_i - a)] \vec{k} \quad (2.1.4)$$

The equation of motion for the i^{th} -mass in vector form is given by:

$$m_i \ddot{\vec{r}}_{I1} = \vec{F}_{g1} + \vec{F}_{T1} + \vec{F}_{p1} \quad (2.1.5)$$

where \vec{F}_{g1} is the gravity force on the i^{th} -mass, \vec{F}_{T1} is the net force due to tether tensions acting upon the same mass and \vec{F}_{p1} is the external perturbation force.

As in Quarterly Report No. 3 the gravitational force is obtained from the potential energy as follows:

$$\vec{F}_{g1} = - \nabla V_i \quad (2.1.6)$$

where V_i is, in this case, given by:

$$V_i = - \frac{1}{2} m_i \Omega^2 [2a^2 + 2az_i - x_i^2 - y_i^2 + 2z_i^2] \quad (2.1.7)$$

Substituting in equation (2.1.6) and performing the derivatives we get:

$$\vec{F}_{g1} = m_i \Omega^2 [-x_i \vec{i} - y_i \vec{j} + (a + 2z_i) \vec{k}] \quad (2.1.8)$$

After substitution of equations (2.1.8) and (2.1.4) into equations (2.1.5) and by assuming (temporarily) $\bar{F}_{pi} = 0$, we finally obtain the three scalar equations of motion for the i^{th} -mass as follows:

$$\begin{aligned}\ddot{x}_i - 2\Omega\dot{z}_i &= F_{Tx_i}/m_i \\ \ddot{y}_i + \Omega^2 y_i &= F_{Ty_i}/m_i \\ \ddot{z}_i - 3\Omega^2 z_i + 2\Omega\dot{x}_i &= F_{Tz_i}/m_i\end{aligned}\tag{2.1.9}$$

The expressions of the tensional forces are as follows:

$$\begin{aligned}F_{Tx_i} &= T_{x_i} - T_{x,i-1} \\ F_{Ty_i} &= T_{y_i} - T_{y,i-1} \\ F_{Tz_i} &= T_{z_i} - T_{z,i-1}\end{aligned}\tag{2.1.10}$$

where the index i is associated with the tether connecting the i^{th} -mass to the $i+1^{\text{th}}$ -mass. In equations (2.1.10) the tension components are as follows:

$$\begin{aligned}T_{x_i} &= T_i (x_{i+1} - x_i)/l_i \\ T_{y_i} &= T_i (y_{i+1} - y_i)/l_i \\ T_{z_i} &= T_i (z_{i+1} - z_i)/l_i\end{aligned}\tag{2.1.11}$$

The tension modulus T_i is given by equation (2.3.13) of Section 2.3 in Quarterly Report No. 3.

In the case of a 4-mass tethered system the 3-dimensional equations of motion, inclusive of three longitudinal dampers placed in series with each tether segment, are finally as follows:

$$\begin{aligned}
\ddot{x}_1 &= 2\Omega\dot{z}_1 + T_1 (x_2 - x_1)/(m_1 l_1) \\
\ddot{x}_2 &= 2\Omega\dot{z}_2 + T_2 (x_3 - x_2)/(m_2 l_2) - T_1 (x_2 - x_1)/(m_2 l_1) \\
\ddot{x}_3 &= 2\Omega\dot{z}_3 - T_2 (x_3 - x_2)/(m_3 l_2) \\
\ddot{y}_1 &= -\Omega^2 y_1 + T_1 (y_2 - y_1)/(m_1 l_1) \\
\ddot{y}_2 &= -\Omega^2 y_2 + T_2 (y_3 - y_2)/(m_2 l_2) - T_1 (y_2 - y_1)/(m_2 l_1) \\
\ddot{y}_3 &= -\Omega^2 y_3 - T_2 (y_3 - y_2)/(m_3 l_2) \\
\ddot{z}_1 &= 3\Omega^2 z_1 - 2\Omega\dot{x}_1 + T_1 (z_2 - z_1)/(m_1 l_1) \\
\ddot{z}_2 &= 3\Omega^2 z_2 - 2\Omega\dot{x}_2 + T_2 (z_3 - z_2)/(m_2 l_2) - T_1 (z_2 - z_1)/(m_2 l_1) \\
\ddot{z}_3 &= 3\Omega^2 z_3 - 2\Omega\dot{x}_3 - T_2 (z_3 - z_2)/(m_3 l_2) \\
T_1 &= k_{t1} (l_1 - l_{d1} - l_{c1}) = k_{t1} l_{t1} \\
T_2 &= k_{t2} (l_2 - l_{d2} - l_{c2}) = k_{t2} l_{t2} \\
T_3 &= k_{t3} (l_3 - l_{d3} - l_{c3}) = k_{t3} l_{t3} \\
\dot{l}_{d1} &= k_{t1} l_{t1}/b_1 - k_1 l_{d1}/b_1 \\
\dot{l}_{d2} &= k_{t2} l_{t2}/b_2 - k_2 l_{d2}/b_2 \\
\dot{l}_{d3} &= k_{t3} l_{t3}/b_3 - k_3 l_{d3}/b_3
\end{aligned} \tag{2.1.12}$$

In equations (2.1.12) $K_{t1} = E_1 A_1 / l_{c1}$ is the stiffness of the i^{th} -tether, l_{t1} is the tether stretch, b_1 is the damping coefficient and k_1 is the stiffness of the i^{th} -longitudinal damper (b_1 and k_1 were called respectively k_{d1} and k_{d1} in Quarterly Report No. 3). The meaning of the other symbols is the same as in Quarterly Report No. 3.

The relations between system quantities $(x_1, \dots, x_n; y_1, \dots, y_n; z_1, \dots, z_n)$ and output/control quantities are derived as in the two-dimensional case. The major difference is that in the 3-dimensional case the lateral displacements of the masses with respect to the line connecting the two end masses have an in-plane and out-of-plane components, respectively called ϵ_{i1} and ϵ_{o1} , and that the out-of-plane libration angle (φ) must be added to the output/control variables. If we call \vec{l}^* the radius vector from m_1 to m_n we have (see Figure 2.1.2):

$$\vec{l}^* = l^* (\cos\varphi \sin\theta \vec{i} + \sin\varphi \vec{j} + \cos\varphi \cos\theta \vec{k}) \tag{2.1.13}$$

We can therefore easily obtain the in-plane (θ) and out-of-plane libration angle (φ) as follows:

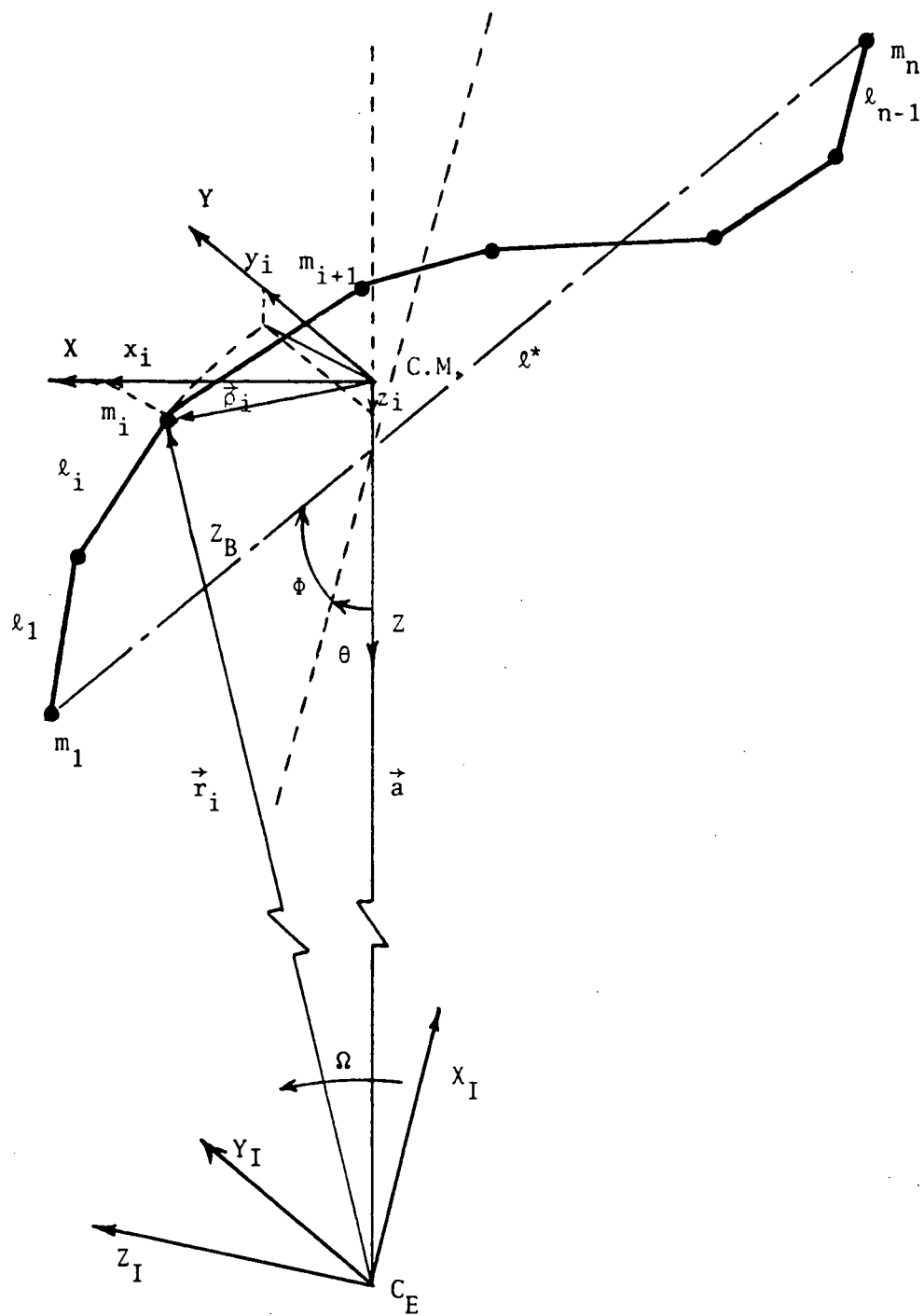


Figure 2.1.2

$$\theta = \operatorname{tg}^{-1} [(x_1 - x_n) / (z_1 - z_n)] \quad (2.1.14)$$

$$\varphi = \sin^{-1} [(y_1 - y_n) / \ell^*]$$

where:

$$\ell^* = [(x_1 - x_n)^2 + (y_1 - y_n)^2 + (z_1 - z_n)^2]^{1/2} \quad (2.1.15)$$

The lateral deflections $\epsilon_1 = [\epsilon_{11}^2 + \epsilon_{01}^2]^{1/2}$ can be obtained by computing the coordinates of the point of intersection between the line through the end masses and its perpendicular through the i^{th} -mass; that is to say by solving the following system of equations:

$$z - z_1 = \frac{1}{m} (y - y_1) = \frac{1}{n} (x - x_1) \quad (2.1.16)$$

$$z - z_1 = m(y - y_1) = n(x - x_1)$$

where:

$$m = (y_1 - y_n) / (z_1 - z_n) \quad (2.1.17)$$

$$n = \operatorname{tg} \theta = (x_1 - x_n) / (z_1 - z_n)$$

By solving equations (2.1.16) we get the coordinates of the intersection point as follows:

$$\begin{aligned}
x_{ci} &= [x_1 - x_{i+1} \operatorname{tg}^2\theta + (z_{i+1} - z_i) \operatorname{tg}\theta] / (1 - \operatorname{tg}^2\theta) \\
y_{ci} &= [y_1 - y_{i+1} m^2 + (z_{i+1} - z_i) m] / (1 - m^2) \\
z_{ci} &= [x_{ci} - x_{i+1}] \operatorname{tg}\theta + z_{i+1}
\end{aligned} \tag{2.1.18}$$

The lateral deflections ϵ_i are therefore given by:

$$\epsilon_i = [(x_{i+1} - x_{ci})^2 + (z_{i+1} - z_{ci})^2 + (y_{i+1} - y_{ci})^2]^{1/2} \quad i = 1, \dots, n-2 \tag{2.1.19}$$

and the in-plane (ϵ_{ii}) and out-of-plane components (ϵ_{oi}) are given by:

$$\begin{aligned}
\epsilon_{ii} &= (\epsilon_{ix}^2 + \epsilon_{iz}^2)^{1/2} \operatorname{sign}(x_{i+1} - x_{ci}) \\
&= [(x_{i+1} - x_{ci})^2 + (z_{i+1} - z_{ci})^2]^{1/2} \operatorname{sign}(x_{i+1} - x_{ci}) \\
\epsilon_{oi} &= \epsilon_{iy} = y_{i+1} - y_{ci}
\end{aligned} \tag{2.1.20}$$

Finally the distance between two contiguous mass points (ℓ_i) is simply given by:

$$\ell_i = [(x_{i+1} - x_i)^2 + (y_{i+1} - y_i)^2 + (z_{i+1} - z_i)^2]^{1/2} \tag{2.1.21}$$

2.2 Software Implementation Of The 3-Dimensional Model And New Integration Subroutine

A new software code has been implemented for the numerical integration of the 3-dimensional model. This software code can handle any tethered system of n masses and $m \leq n-1$ longitudinal dampers (in series with the tether segments). The location of the longitudinal dampers may be anywhere and must be specified by the user. Additional subroutines provide the control laws for reeling in and out the tethers connecting the various platforms.

The output of the computer code has been modified in order to accommodate the greater number of variables to be plotted. Moreover a subroutine has been written for formatting one of the output files in the format suitable for the graphic software of SKYHOOK. The computer code can therefore produce the familiar side-view and front-view of the constellation shape by plotting sequential shots at a specified interval of time. A new integration subroutine has also been added as an option to the variable step, IV-order Runge-Kutta. The Runge-Kutta subroutine is a very stable subroutine the only drawback of which is the introduction of an artificial numerical damping¹ when long integration step size are adopted. The new integrator is a variable step (constant relative accuracy) predictor-corrector, initialized by a Runge-Kutta subroutine. The predictor-corrector is recommended in reference [1] over the Runge-Kutta, the Gear and other integration subroutines as the one that provides the best compromise among stability, speed and accuracy, especially for non-linear equations. We have compared the predictor-corrector subroutine to the IV-order Runge-Kutta on a test case simulation run of the 4-mass tethered system. When we adopted a relative accuracy of 10^{-6} (which produces good results with the Runge-Kutta subroutine) the two integration subroutines produced exactly the same results. The predictor-corrector subroutine, however, has been 40% faster than the Runge-Kutta, proving its advantage over the latter. The Runge-Kutta did not show any artificial numerical damping for relative accuracy better or equal to 10^{-6} .

References to Section 2.2

1. D'Souza, A.F. and V.K. Garg, "Advanced Dynamics, Modeling and Analysis." Prentice Hall, 1984.

2.3 Simulation Runs Of The Station Keeping Phase Of The 4-Mass Tethered System With/Without Longitudinal Dampers

The new computer code that models the dynamics of n-mass, 3-dimensional tethered systems has been used to simulate the dynamic response of a 4-mass tethered system. The system under investigation, depicted in Figure 2.3.1, consists of : the Space Station with a mass $m_2 = 306.752$ metric tons located at the C.M. of the system, an end mass, $m_4 = 10$ metric tons, deployed upward on a 10 km long, 2 mm diameter kevlar tether, a variable-g platform (m_3) of 5 metric tons that can crawl along the upward tether segment and a balancing mass, $m_1 = 10$ metric tons deployed downward on a 10-15 km tether of the same material and shape as the upward tether. The tether length (l_1) of tether no.1 can be adjusted in such a way as to maintain the C.M. of the entire system at the desired vertical location on board the Space Station. In the following simulation runs of this quarterly report the variable-g platform (m_3) is arbitrarily placed at a distance of 1 km from the Space Station on the upper tether segment. The dynamic response of the system has been simulated during the station-keeping phase. The first simulation has been run, without any passive and/or active dampers, starting from a perturbed initial state of the system. The initial in-plane libration angle of the system is 0.51° while the initial out-of-plane angle is 0.42° . The initial lateral deflections of mass m_2 (Space Station) and m_3 (variable-g laboratory) with respect to the line through the end masses are respectively as follows: $\epsilon_{11} = -89.m$, $\epsilon_{12} = 93.m$ (in plane components); $\epsilon_{01} = -73.m$, $\epsilon_{02} = -56.m$ (out-of-plane components); $l_1 = 10500.m$, $l_2 = 1000.m$, $l_3 = 9000.m$. The reason for having some numbers which are not perfectly round in the initial conditions is that the initial conditions are supplied to the computer code in terms of the masses' Cartesian coordinates. The Cartesian coordinates, however, do not provide an immediate picture of the system configuration;

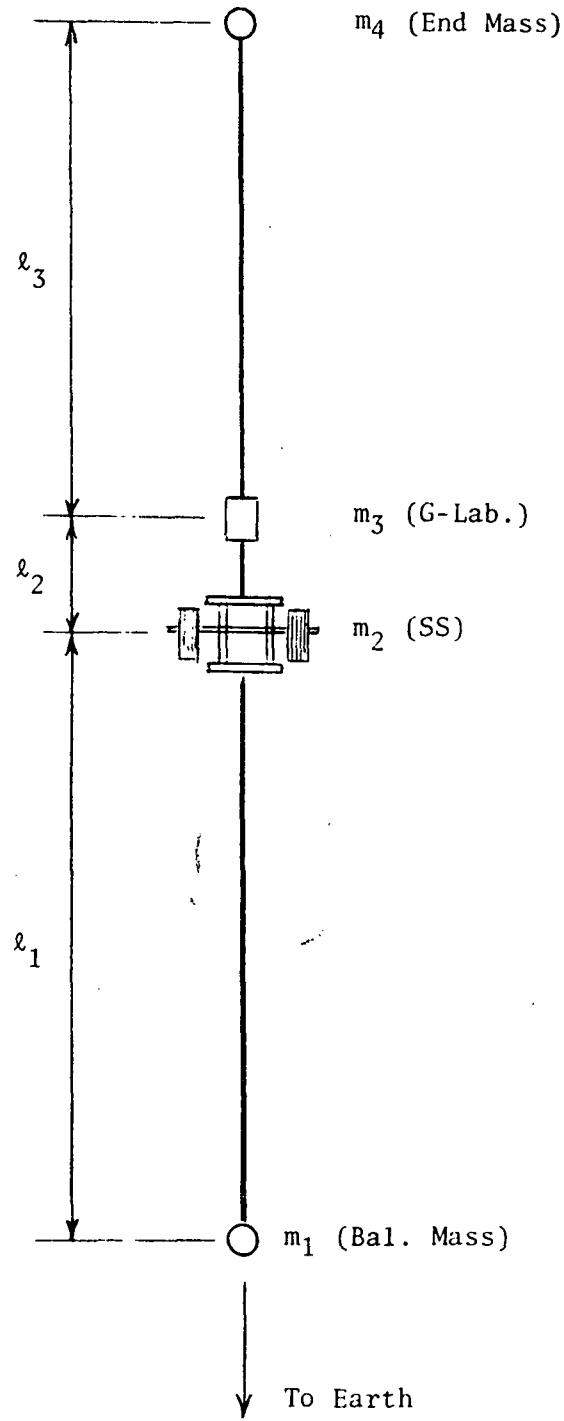


Figure 2.3.1

which is better represented by coordinates like θ , φ , ϵ 's and l 's.

The following set of plots, shown in Figure 2.3.2a-x, has been obtained by simulating for 7200.sec the undamped response of the system due to the perturbed initial conditions previously described. The in-plane and out-of-plane libration angles are plotted in Figure 2.3.2a. The oscillation periods are $T_\theta \simeq 3240$.sec and $T_\varphi \simeq 2810$.sec respectively, which correspond to the undamped, free oscillation angular frequency of $\sqrt{3}\Omega$ and 2Ω respectively, where $\Omega = 1.119 \times 10^{-3}$ rad/sec at 450 km of altitude. Figures 2.3.2b and c show the phase-planes $\theta = \dot{\theta}$ and $\varphi = \dot{\varphi}$ respectively. These two plots clearly show the undamped response of the in-plane and out-of-plane libration and the small effects due to the lateral vibrations of the masses that are depicted by the small wiggles superimposed to the elliptical graphs. Figure 2.3.2d,e and f depict the tether lengths of tethers no.1, 2 and 3 respectively. The shape of the plots is due to the superimposition of the longitudinal, lateral and librational frequencies that all affect the tether lengths plus beating phenomena. The highest oscillation frequency is the longitudinal frequency in tether no.2, the shortest tether and therefore the stiffest. The in-plane components of the lateral displacements ϵ_{11} and ϵ_{12} , respectively of mass m_2 and m_3 , are shown in Figure 2.3.2g; while the out-of-plane components ϵ_{01} and ϵ_{02} are shown in Figure 2.3.2h. Figure 2.3.2i shows the moduli of the lateral displacements (ϵ_1) and (ϵ_2); the decrease in amplitude is due only to a beating phenomenon between the components and is not due to damping. Figures 2.3.2j and k are the phase-planes $\epsilon_1 - \dot{\epsilon}_1$ and $\epsilon_2 - \dot{\epsilon}_2$ respectively. The decrease in amplitude is again due to a beating phenomenon. The tether tensions of tethers no.1, 2 and 3 are depicted in Figures 2.3.2l, m and n respectively. The shapes of these plots are exactly like those of the associated tether lengths since the tension is proportional to the tether stretch, the tether lengths at rest are constant and there are no longitudinal

dampers. Figure 2.3.2p shows the flight-direction (ACH), transverse (ACL) and vertical component (ACV) respectively of the acceleration, at the C.M. of the Space Station, induced by the transient dynamics of the system. The level of acceleration, shown in the figure, is only due to the initial conditions and may be theoretically reduced to zero by a perfect damping system. A large section of the study of the 4-mass system will be devoted to the damping of the various vibrational modes of the system and the effect of the external perturbations on the acceleration level. Figure 2.3.2p clearly shows the contribution of the various vibrational modes to the acceleration components. The acceleration components at the variable-g laboratory (m_3) are shown in Figures 2.3.2q, r and s respectively. It is clear from the figures that the flight-direction and transverse components are primarily due to the lateral oscillations of mass m_3 , while the vertical component is affected by various vibrational modes. The vertical component also shows the bias due to the 1 km distance from the system C.M. Figure 2.3.2s t, u and v are the familiar SKYHOOK-type plots. In these plots the shape of the system, at time intervals of 20 sec for 3600 sec, is depicted as seen from the side (radial/in-plane) in Figure 2.3.2t and from the front (radial/out-of-plane) in Figure 2.3.2u. The scale of the abscissa is largely expanded in order to show the otherwise undetectable oscillations. The overall length of the system is also normalized. The mass numbering is the same adopted in Figure 2.3.1 so that the Space Station is mass no. 2. The Earth is therefore on the side of mass no. 1 in the direction of the positive ordinates. Without the expansion of the scale of the abscissa the former plots look like Figure 2.3.2v, that is the equal-scale side-view of the system plotted every 20 sec for 1000 sec only.

The first stage of damping is implemented into the system by adding three longitudinal dampers in series with the three tether segments. Each damper is

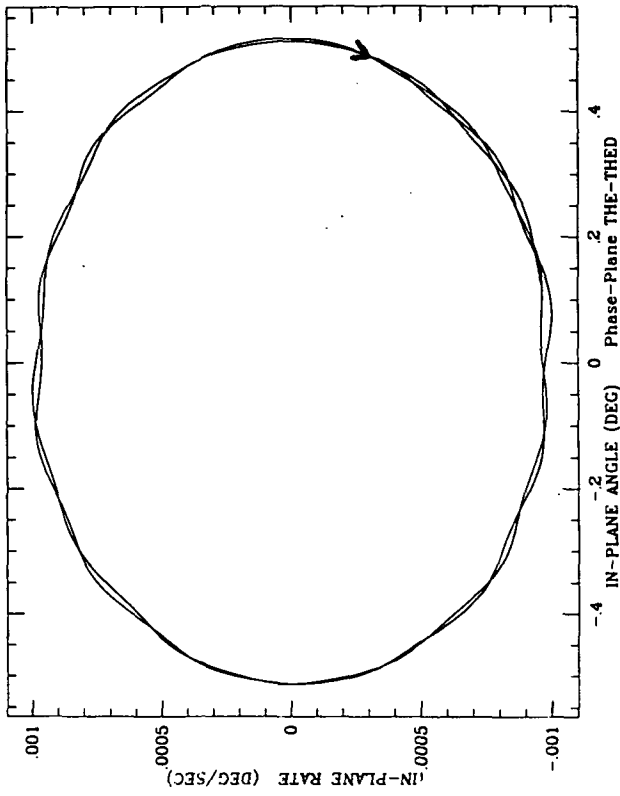


Figure 2.3.2a

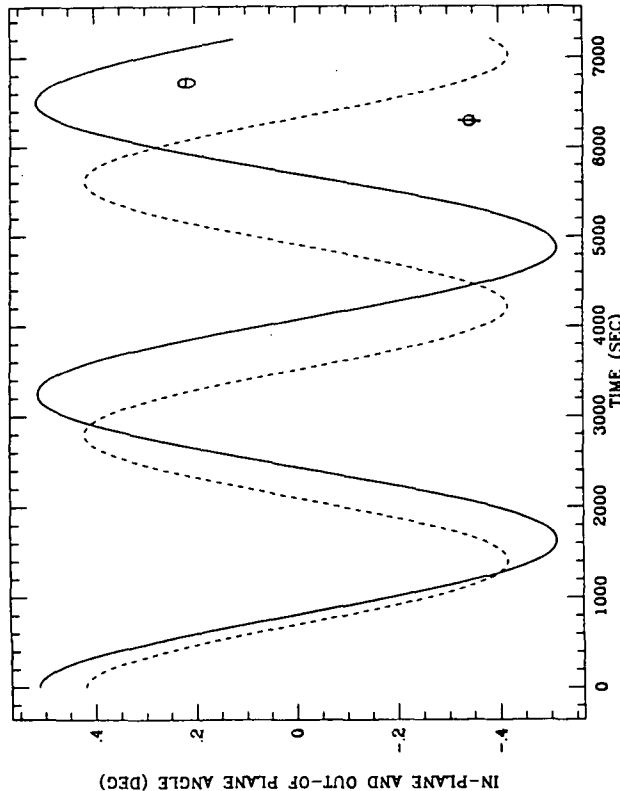


Figure 2.3.2b

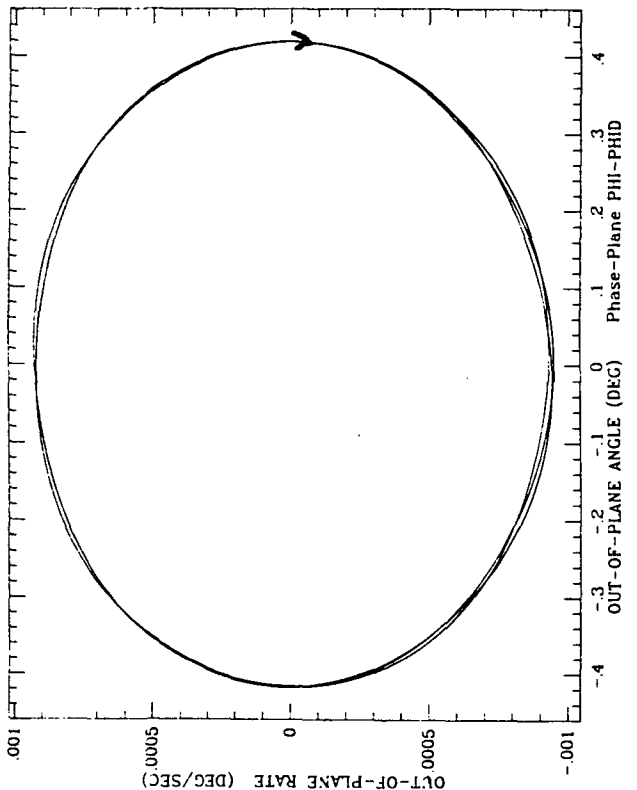


Figure 2.3.2c

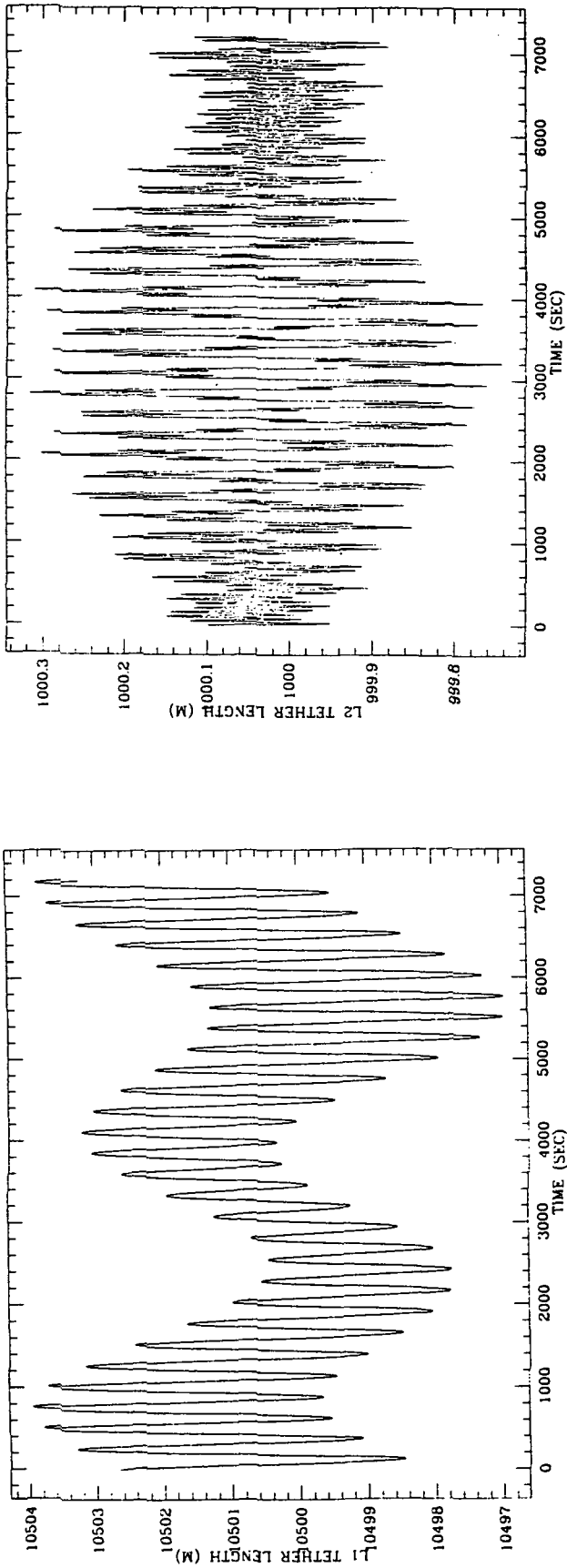


Figure 2.3.2d

Figure 2.3.2e

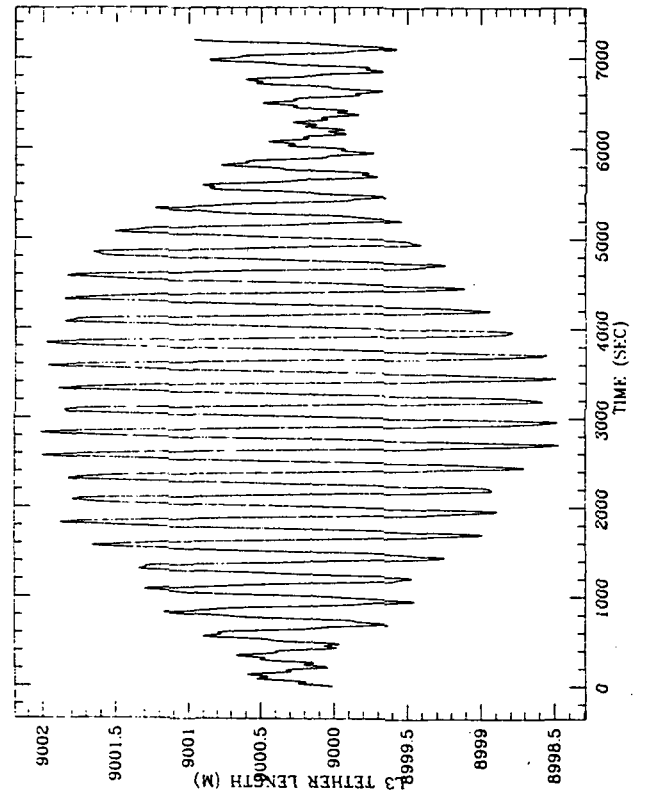


Figure 2.3.2f

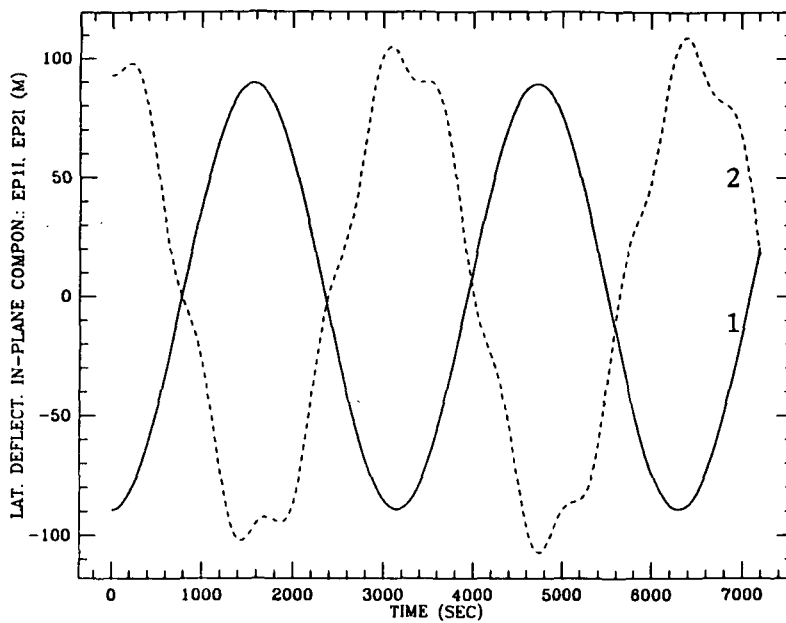


Figure 2.3.2g

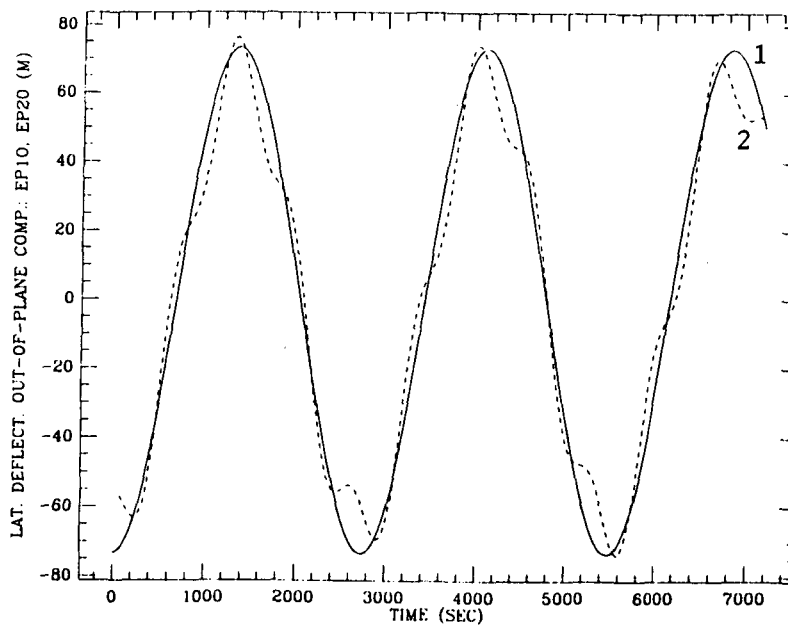


Figure 2.3.2h

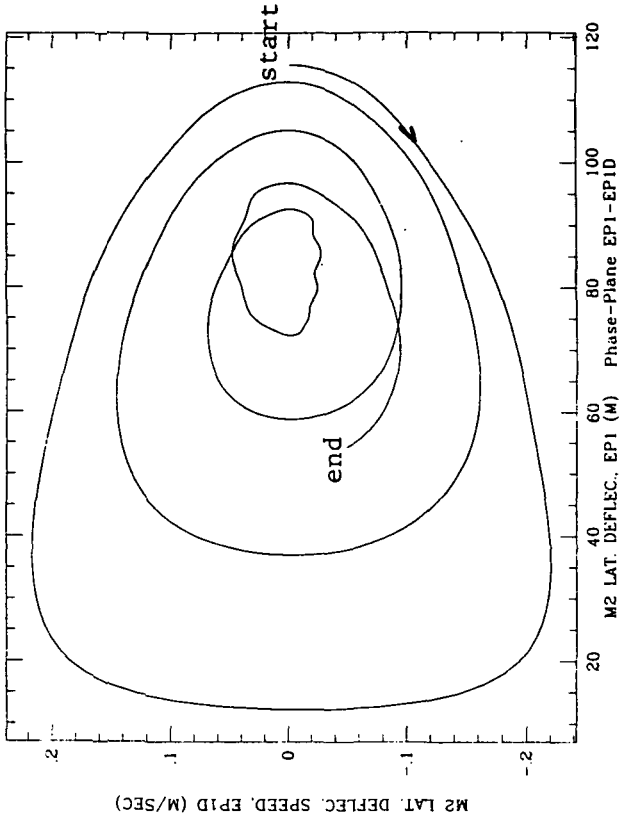


Figure 2.3.2j

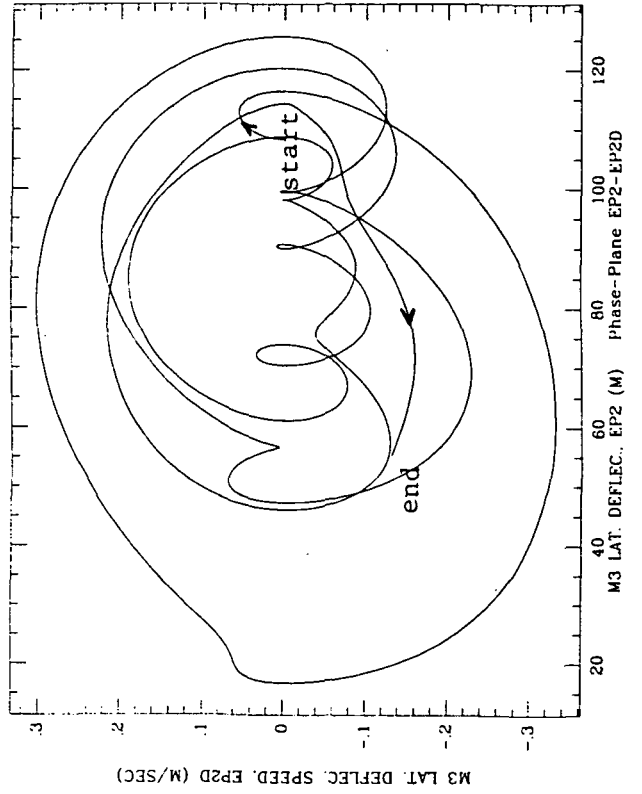


Figure 2.3.2k

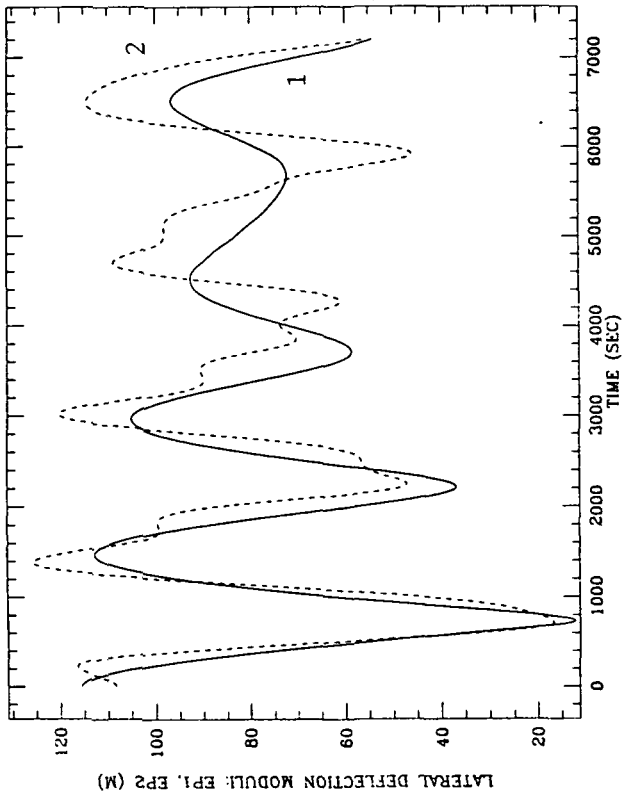


Figure 2.3.2i

ORIGINAL PAGE IS
OF POOR QUALITY

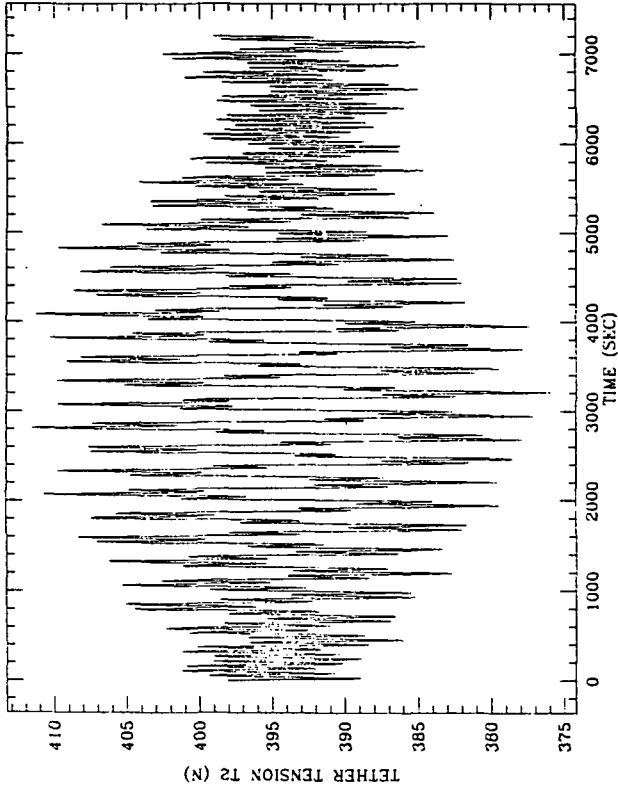


Figure 2.3.2m

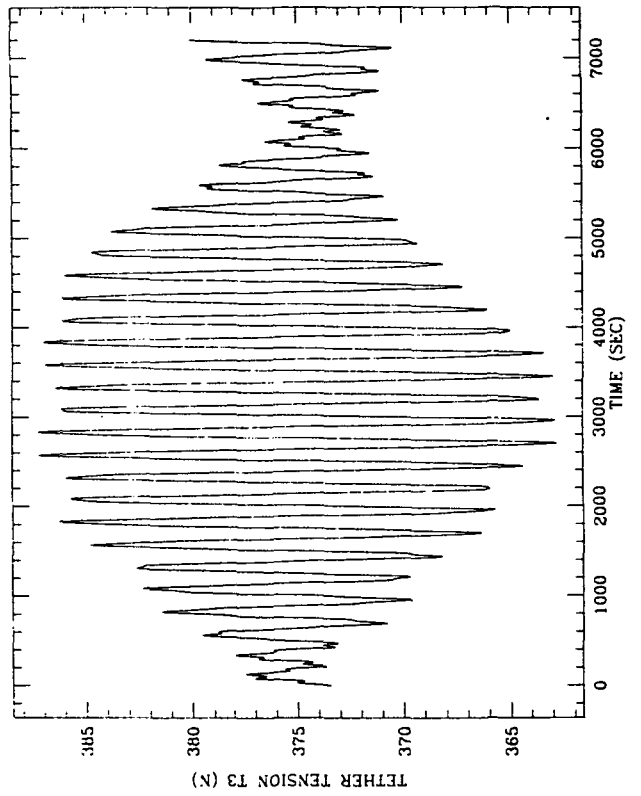


Figure 2.3.2n

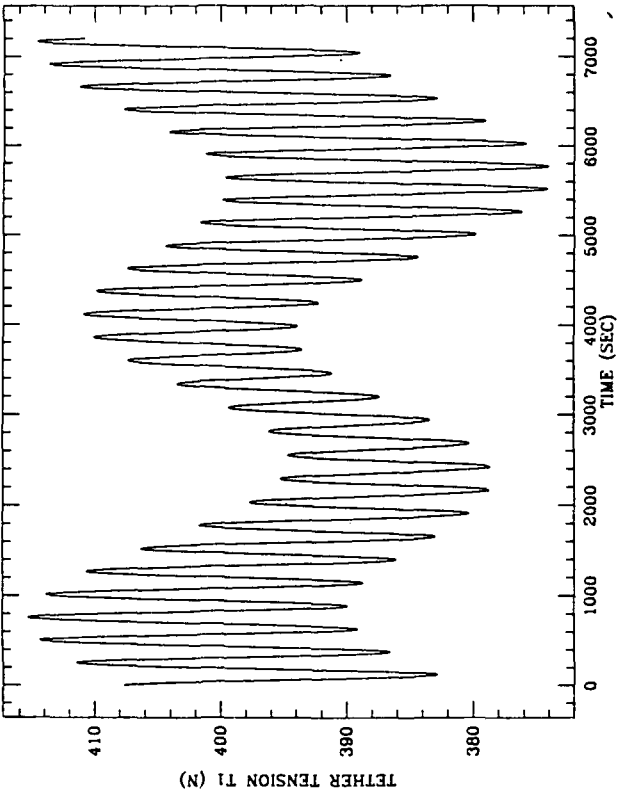


Figure 2.3.2l

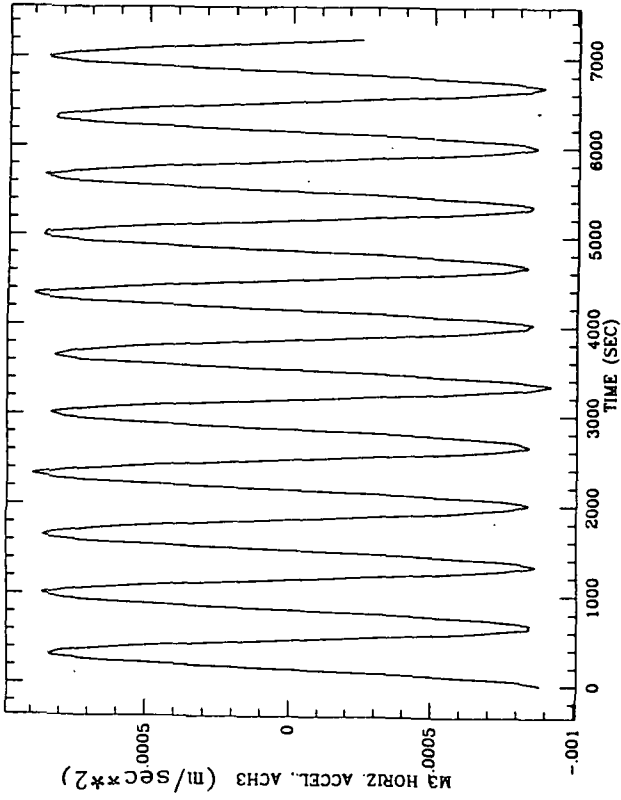


Figure 2.3.2q

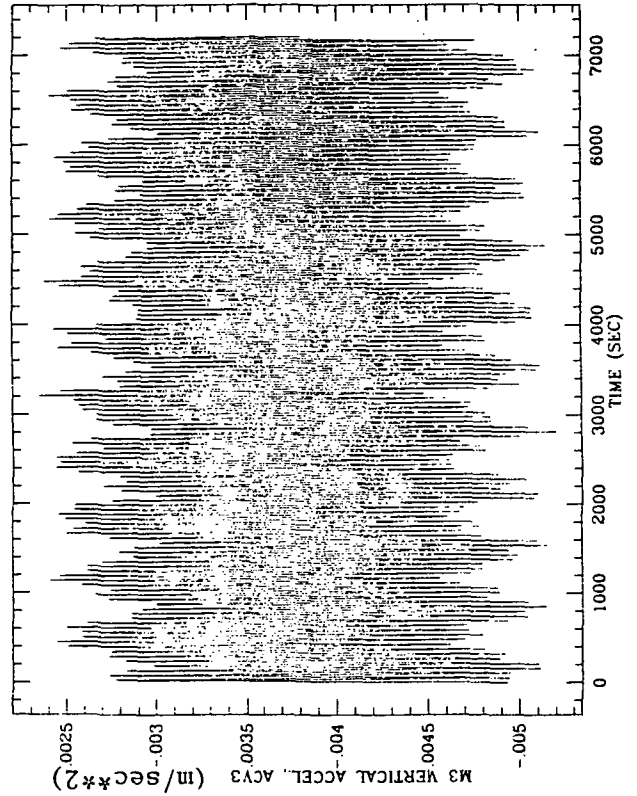


Figure 2.3.2s

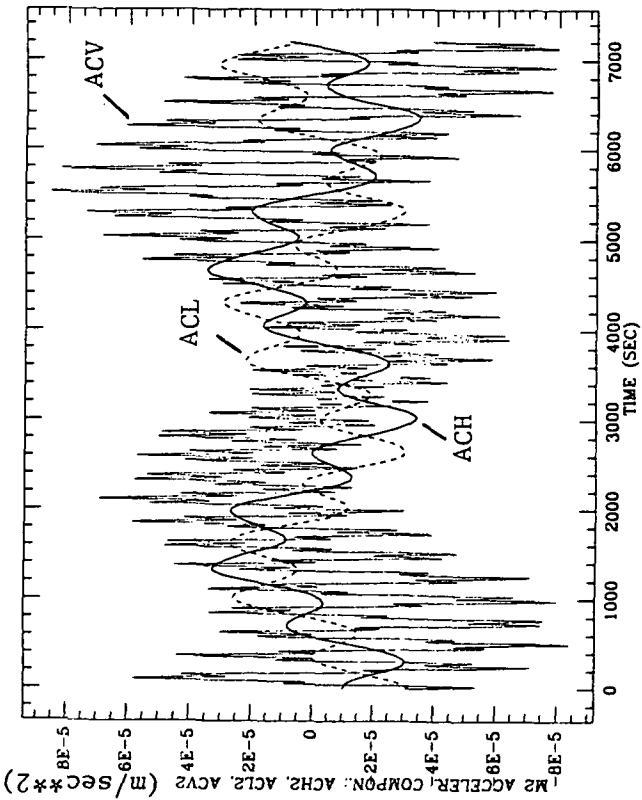


Figure 2.3.2p

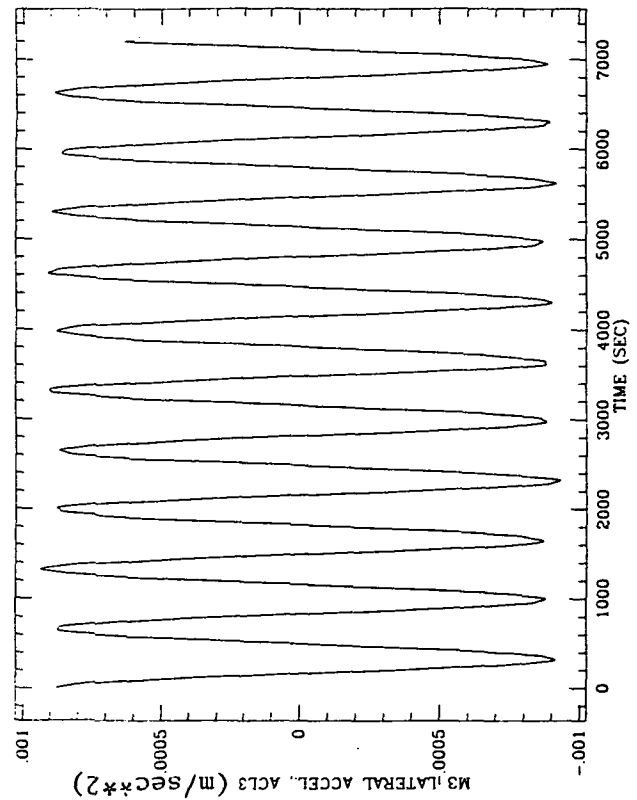


Figure 2.3.2r

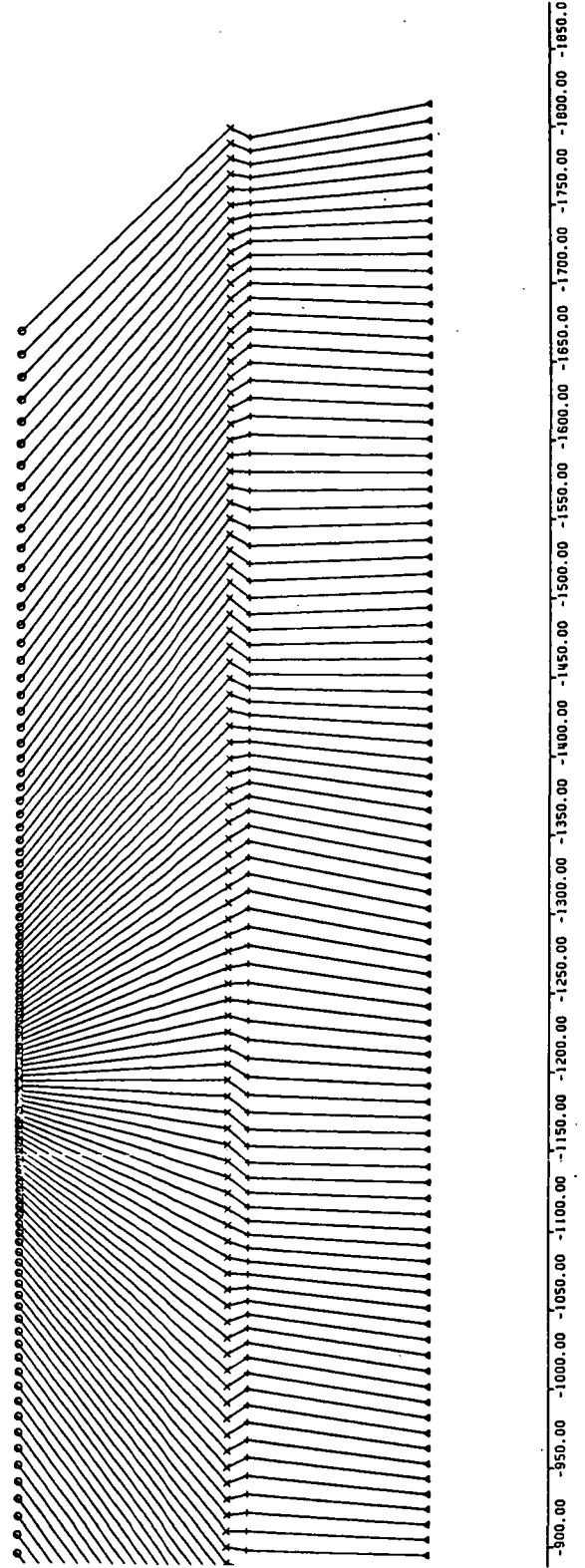
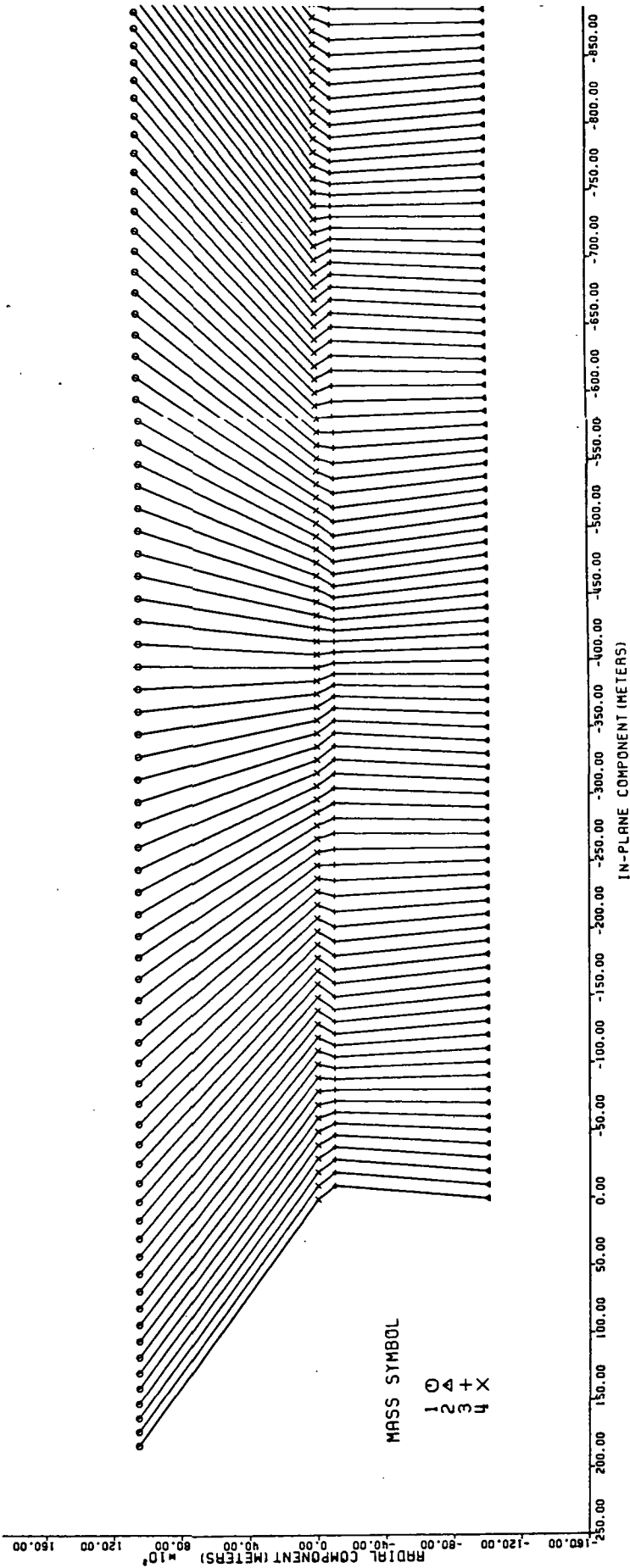


Figure 2.3.2t - Expanded Scale, Side-View Plotted Every 20 Sec for 3600 Sec. No Dampers.

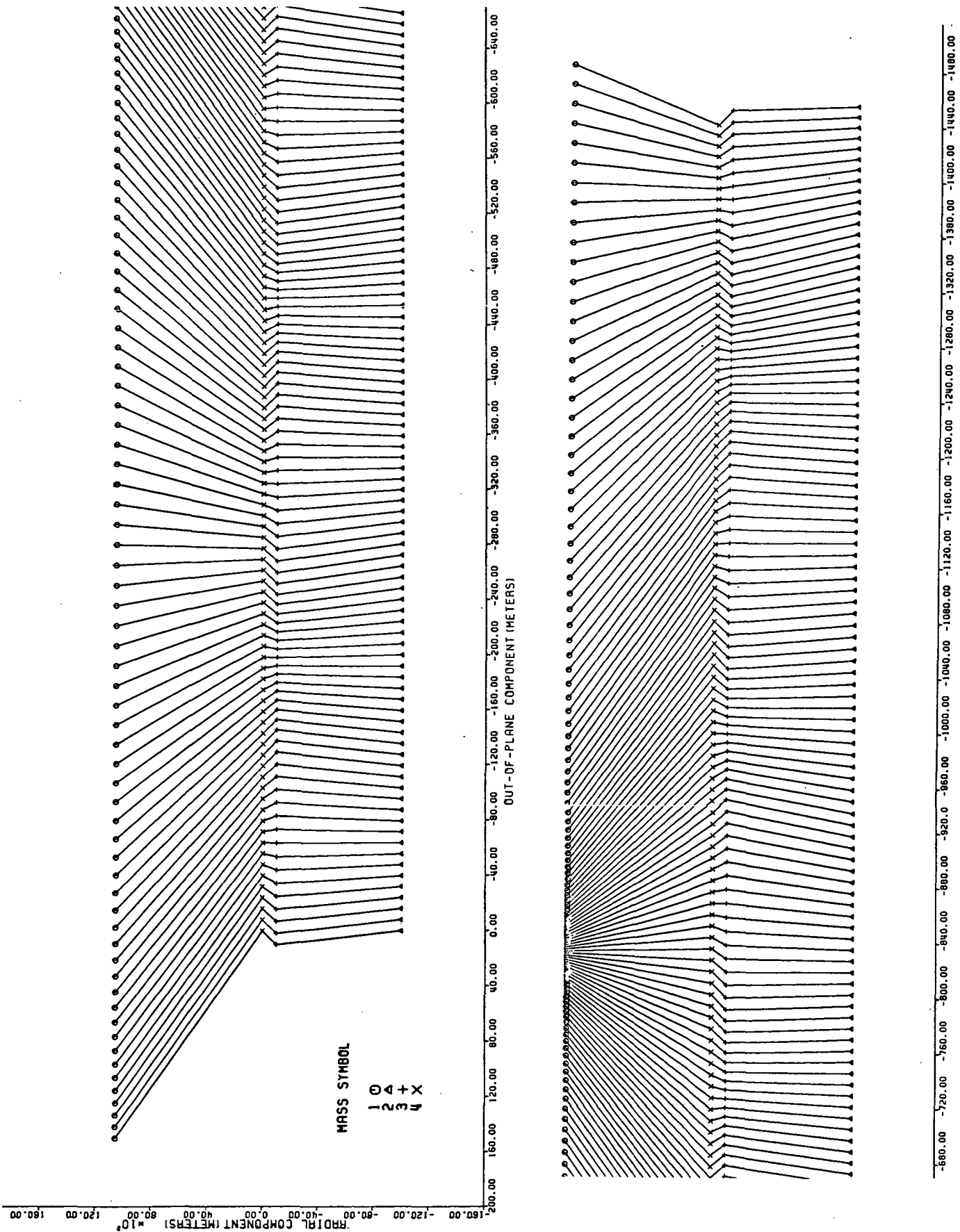


Figure 2.3.2u - Expanded Scale, Front-View Plotted Every 20 Sec for 3600 Sec. No Dampers.

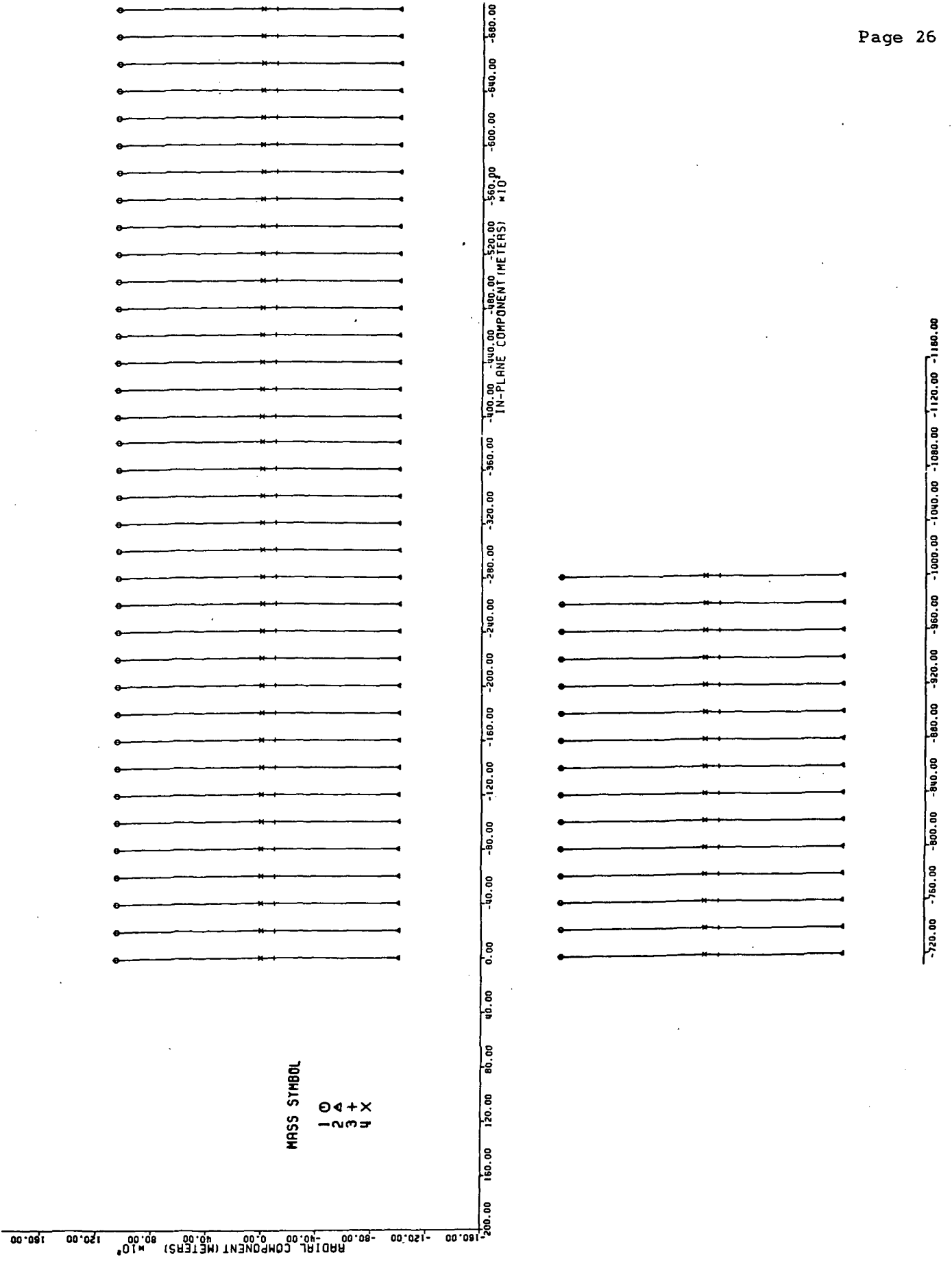


Figure 2.3.2v - Equal Scale, Side-View Plotted Every 20 Sec for 1000 Sec. No Dampers.

tuned to the frequency of the associated, single degree of freedom, oscillating system (associated tether plus the two masses at that tether's tips) and the damping coefficient is selected in order to achieve a damping ratio of approximately 0.9. The dramatic positive effect of the longitudinal dampers upon the longitudinal oscillatory modes is shown in Figure 2.3.3a-m. The time histories of the libration angles θ and φ and the lateral displacements ϵ_1 and ϵ_2 are negligibly influenced by the longitudinal dampers and they are, therefore, very similar to the respective plots of the previous simulation run. The tether lengths of tethers no.1, 2 and 3, for the system with longitudinal dampers, are shown in Figure 2.3.3a, b and c. These figures must be compared with Figures 2.3.2d, e and f respectively of the previous run. The longitudinal dampers abate very effectively the higher frequency longitudinal oscillation modes but are not effective against the longitudinal oscillation forced by lateral and/or librational oscillations. Figures 2.3.3d, e and f, depicting the tension in tethers no. 1, 2 and 3 respectively, must be compared to Figures 2.3.2l, m and n. Similar considerations to those pointed out for the tether lengths apply to these tension plots. Figures 2.3.3g, h and i show the lengths of the longitudinal dampers associated to tethers no. 1, 2 and 3 respectively. Since each longitudinal damper is tuned to the frequency of the associated tether, the length of each longitudinal damper is equal to the elastic stretch of the associated tether. The acceleration components ACH (flight-direction), ACL (transverse) and ACV (vertical) on board the Space Station are shown in Figure 2.3.3j. By comparing Figure 2.3.3j with Figure 2.3.2p it is clear that the vertical component of the acceleration is the most affected by the longitudinal dampers; its amplitude is reduced and it becomes comparable to the other two components. Figures 2.3.3k, l and m show the acceleration components on board the variable-g laboratory. The flight-direction component and the transverse component are almost identical to those shown in Figures 2.3.2q and r of the previous simula-

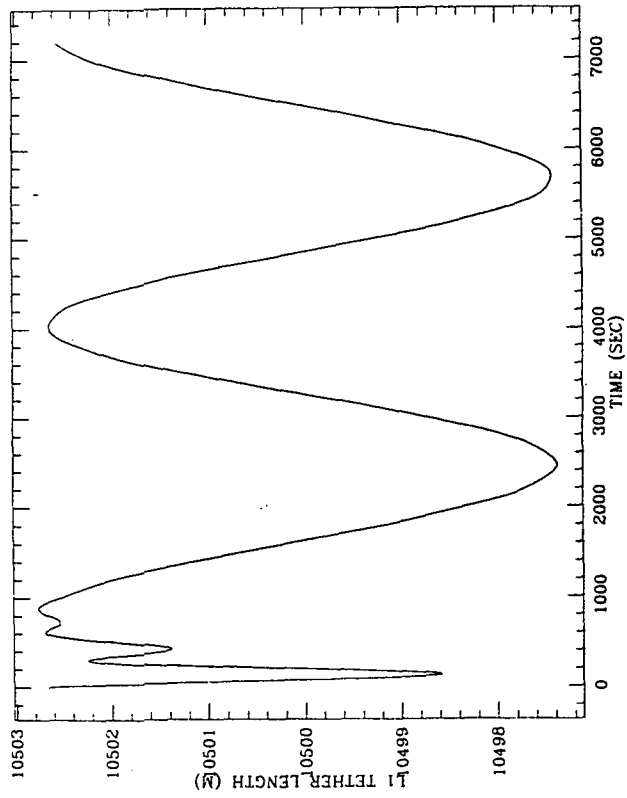


Figure 2.3.3a

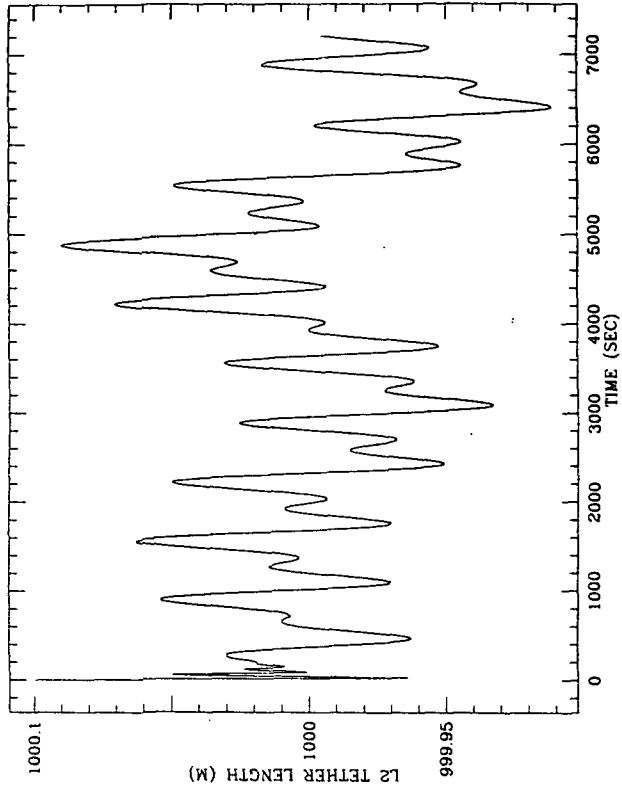


Figure 2.3.3b

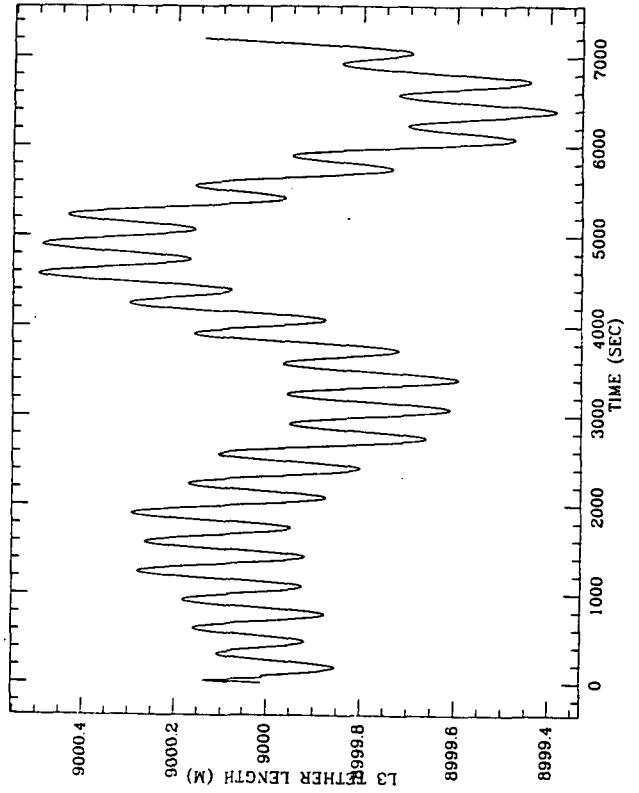


Figure 2.3.3c

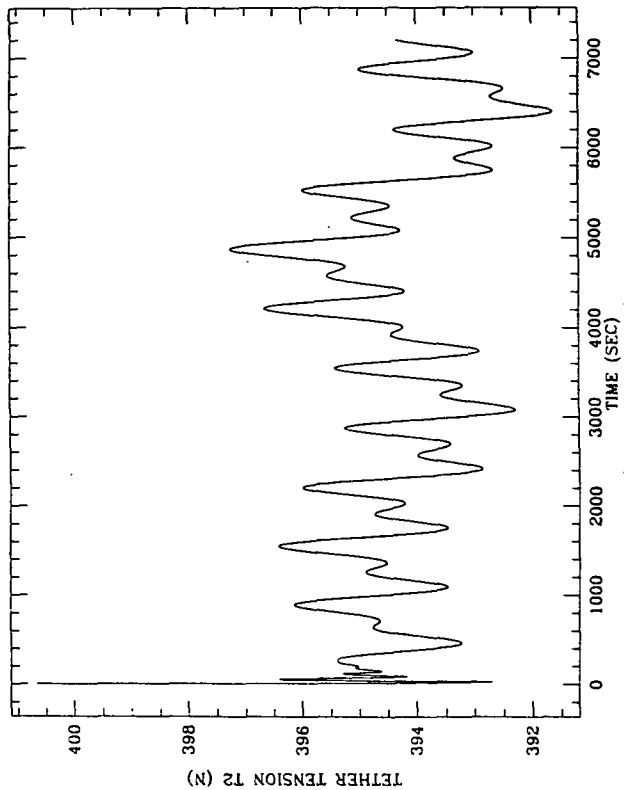


Figure 2.3.3e

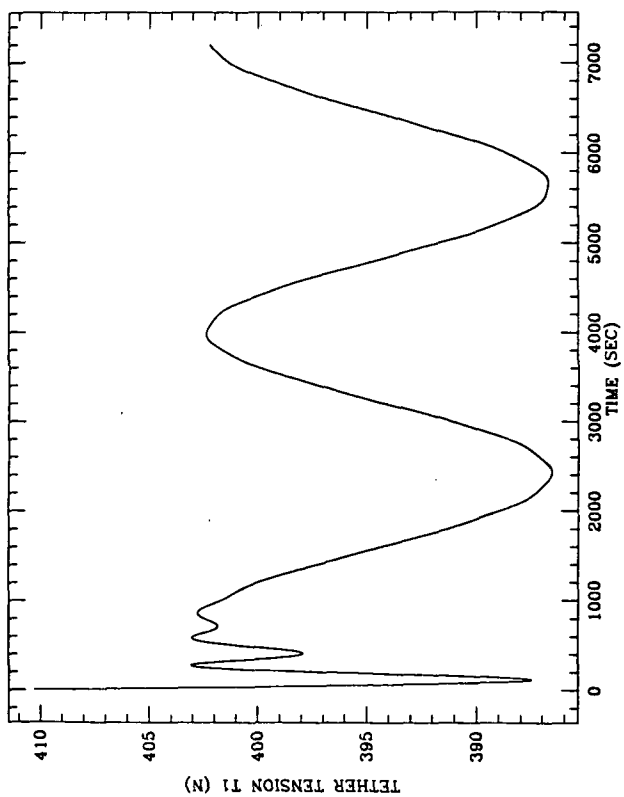


Figure 2.3.3d

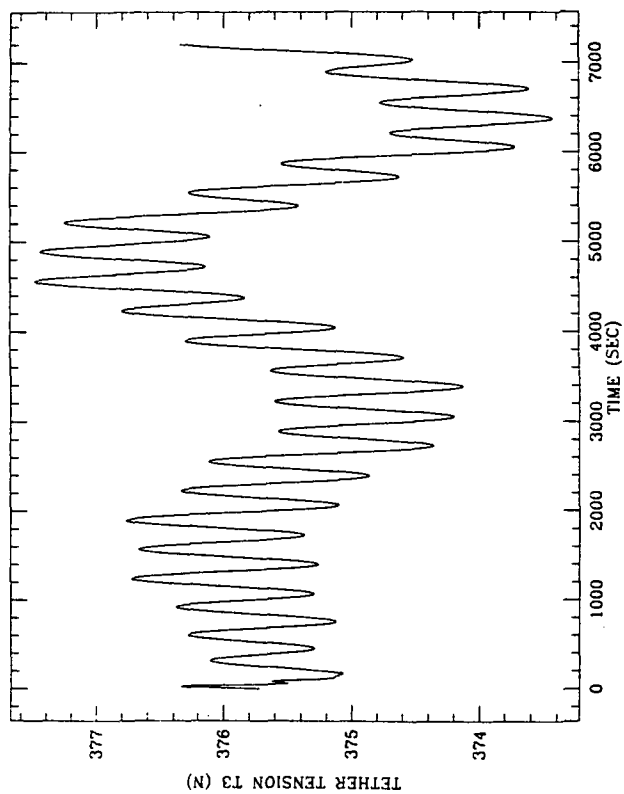


Figure 2.3.3f

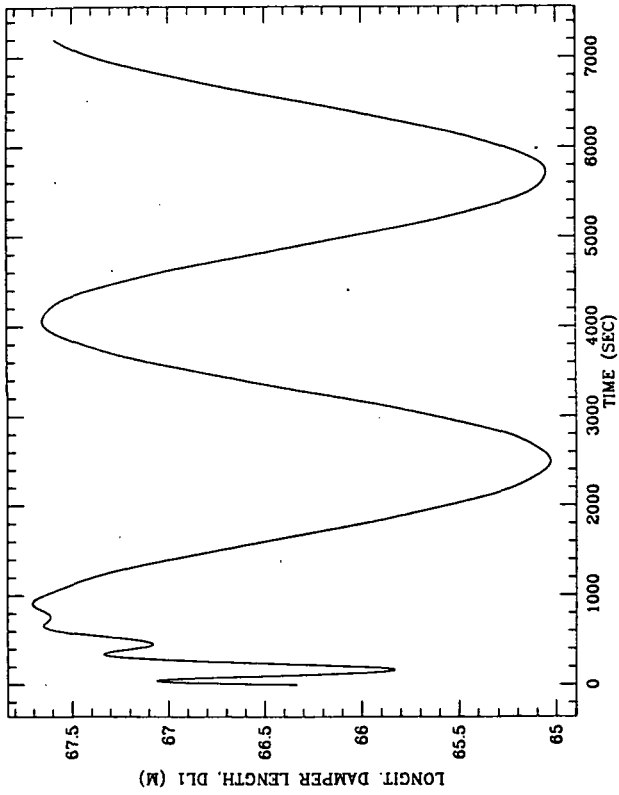


Figure 2.3.3g

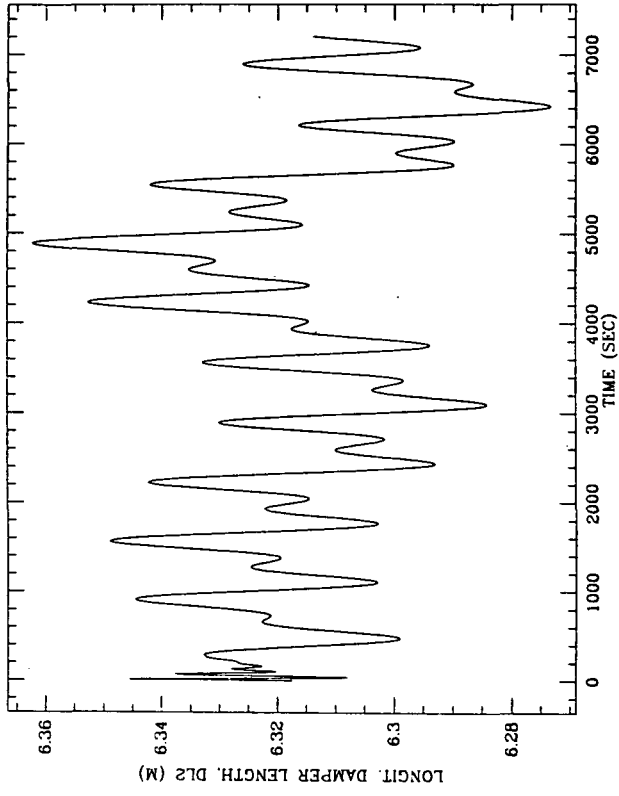


Figure 2.3.3h

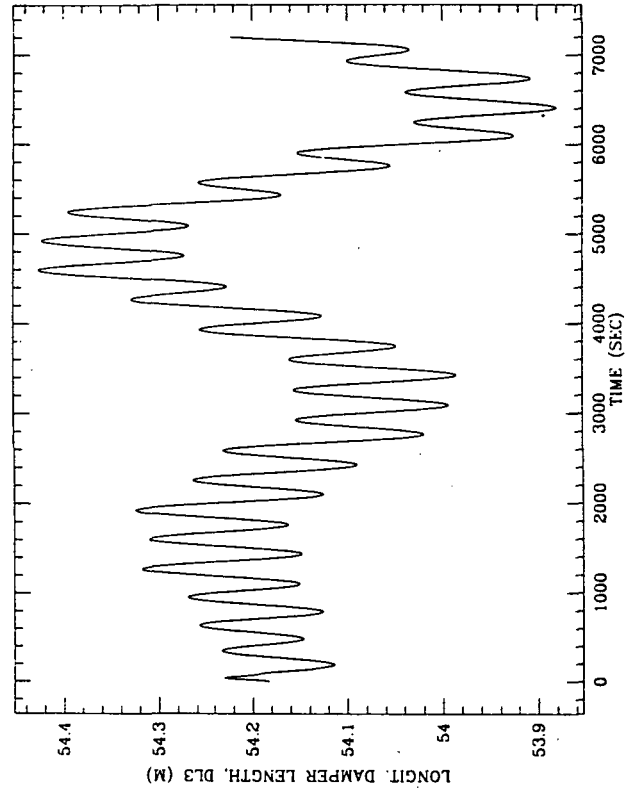


Figure 2.3.3i

ORIGINAL PAGE IS
OF POOR QUALITY

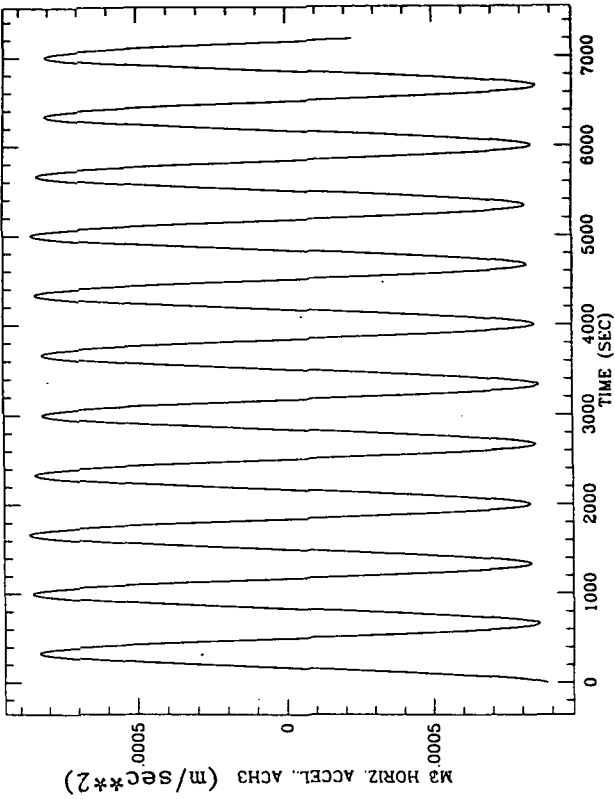


Figure 2.3.3k

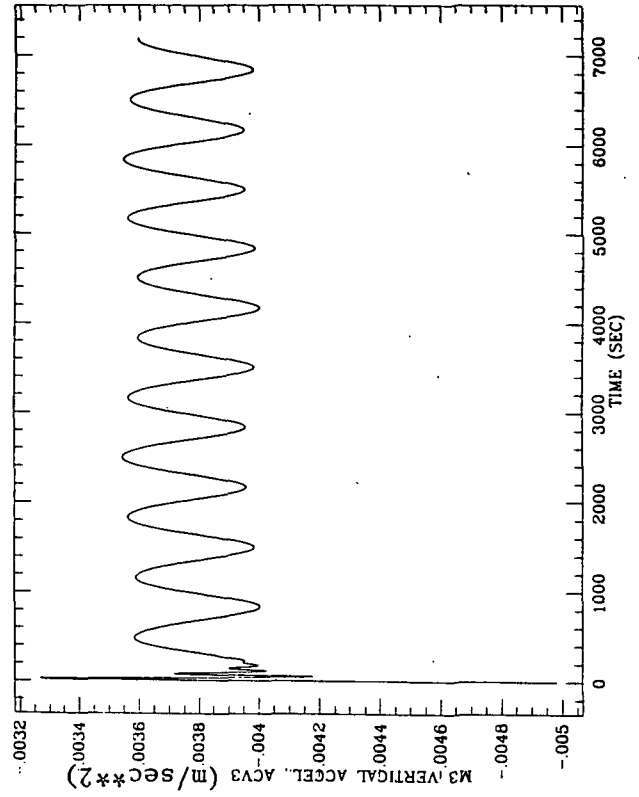


Figure 2.3.3m

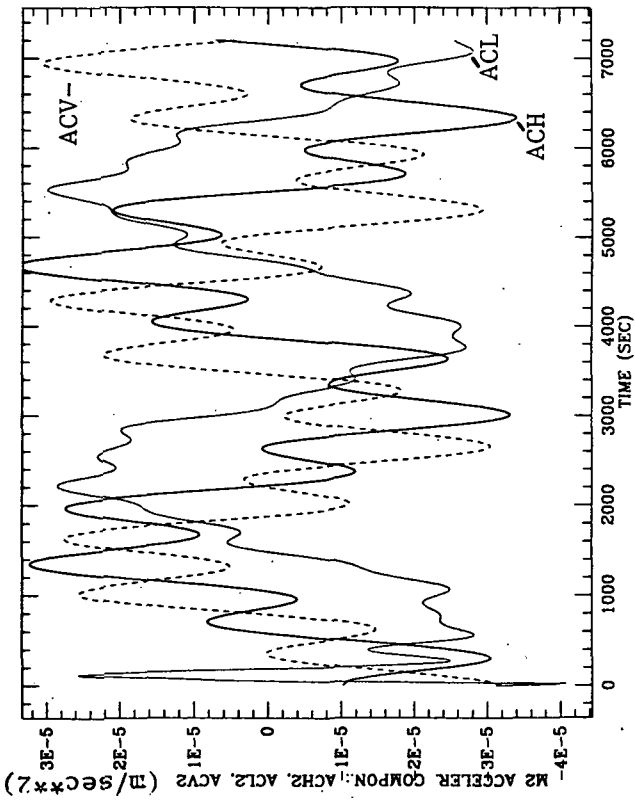


Figure 2.3.3j

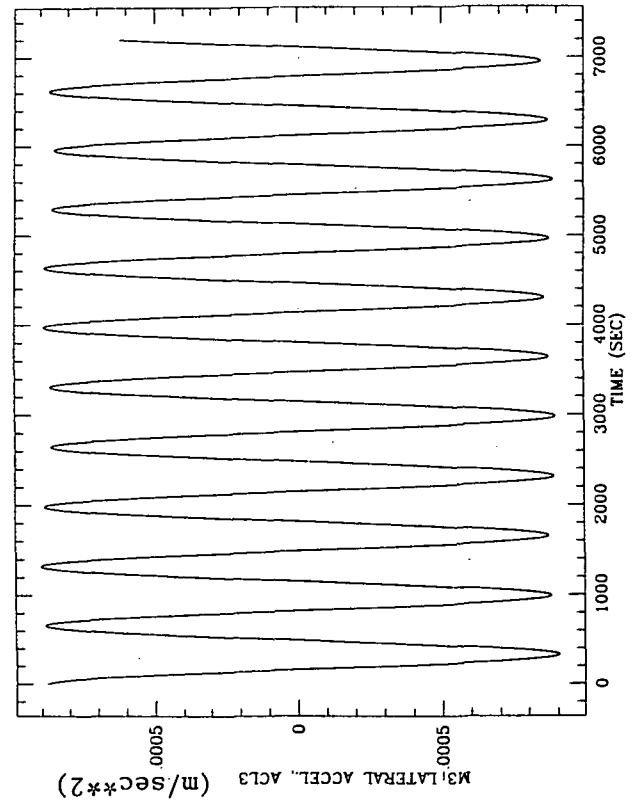


Figure 2.3.3l

tion. The vertical component is on the contrary positively affected by the longitudinal dampers (compare with Figure 2.3.2s); the higher frequency components have been abated and the acceleration level is closer to the steady state value. Since the side-view and the front-view of the system (SKYHOOK-type plots) are negligibly affected by the longitudinal dampers, they are not shown in this simulation run.

2.4 Damping Algorithms For In-Plane Librational And Lateral Oscillatory Modes

The damping algorithms for the in-plane librational and lateral oscillatory modes have been devised by generalizing and modifying the damping algorithms derived in Quarterly Report No. 2 for the 3-mass, 2-dimensional model.

In-Plane Libration Damping Algorithms

In Section 2.3 of Quarterly Report No. 2 it is shown that a 3-mass tethered system librates about the system C.M. Since the libration frequency is independent of the mass and its distance from the system C.M., the statement above can be generalized to an n-mass system. In order to maintain the Space Station (m_2) at the system C.M. while the in-plane libration damping algorithm is active, the tether lengths must be controlled with a control law similar to equation (2.3.3) of Quarterly Report No. 2. The in-plane libration damping algorithm for the 4-mass tethered system is therefore formulated as follows:

$$\begin{aligned}
 l_{1c} &= l_{01} (1 - k_{\theta}\theta) \\
 l_{2c} &= l_{02} (1 - k_{\theta}\theta) \\
 l_{3c} &= l_{03} (1 - k_{\theta}\theta)
 \end{aligned}
 \tag{2.4.1}$$

where l_{01} , l_{02} and l_{03} are the steady state values of the tether lengths.

In-Plane Lateral Oscillation Damping Algorithms

The damping of the in-plane lateral oscillatory modes is obtained with a technique similar to that adopted in Section 2.3 of Quarterly Report No. 2. Note that in the above mentioned report the signs in front of the terms in ϵ in equations (2.3.5) and (2.3.6) are misprinted and should be inverted. The damping of lateral oscillations is obtained by moving the two middle masses, m_2 and m_3 (by controlling the tether lengths) in such a way as to produce Coriolis forces opposed to the lateral displacements of the middle masses (negative work). The tether control laws for the damping of the in-plane lateral oscillations are, when expressed in terms of tether length variations, as follows:

$$\begin{aligned}
 \Delta l_{1c} &= k_{\epsilon 11} \epsilon_{11} \\
 \Delta l_{2c} &= k_{\epsilon 12} \epsilon_{12} l_{02} / l_{03} - k_{\epsilon 11} \epsilon_{11} \\
 \Delta l_{3c} &= -k_{\epsilon 12} \epsilon_{12} l_{02} / l_{03}
 \end{aligned}
 \tag{2.4.2}$$

where $k_{\epsilon 11}$ and $k_{\epsilon 12}$ are the gains for the lateral oscillation in-plane components ϵ_{11} and ϵ_{12} respectively.

By assuming a linear superimposition of effects, equations (2.4.2) must be added to equations (2.4.1) in order to obtain the tether length control laws which provide in-plane libration and lateral oscillation damping. The final result is as follows:

$$\begin{aligned}
 l_{1c} &= l_{01} (1 - k_{\theta}\theta + k_{\epsilon 11}\epsilon_{11}/l_{01}) \\
 l_{2c} &= l_{02} (1 - k_{\theta}\theta + k_{\epsilon 12}\epsilon_{12}/l_{03} - k_{\epsilon 11}\epsilon_{11}/l_{02}) \\
 l_{3c} &= l_{03} (1 - k_{\theta}\theta - k_{\epsilon 12}\epsilon_{12}l_{02}/l_{03}^2)
 \end{aligned}
 \tag{2.4.3}$$

Equations (2.4.3) are adopted in the next section as damping algorithms for the in-plane libratory modes of the system.

2.5 Station-Keeping Simulation Runs With/Without Librational And Lateral Damping Algorithms

A third simulation run, similar to the second simulation of this report, but with different initial conditions, has been made. In the third run the 4-mass system is modeled like in simulation no. 2 (with longitudinal dampers only). The third run, however, differs from the second because the initial conditions of the third run are 90° out-of-phase with respect to run no. 2 (the initial velocities are different from zero in run no. 3). The initial conditions of simulation no. 3 are therefore as follows: $\dot{\theta} = 4.7 \times 10^{-4}$ deg/sec, $\dot{\varphi} = 3.9 \times 10^{-4}$ deg/sec, $l_1 = 10500$.m, $l_2 = 1000$.m, $l_3 = 9000$.m, $l_{d1} = 66.33$ m, $l_{d2} = 6.32$ m, $l_{d3} = 54.18$ m (where l_d 's are the lengths of the longitudinal dampers), $\dot{\epsilon}_{11} = -8.33 \times 10^{-2}$ m/sec, $\dot{\epsilon}_{12} = -3.38 \times 10^{-2}$ m/sec, $\dot{\epsilon}_{01} = -6.83 \times 10^{-2}$ m/sec, $\dot{\epsilon}_{02} = -1.91 \times 10^{-1}$ m/sec, all the other variables are initially set equal to zero. Figures 2.5.1a-za show the dynamic response of the system over a time of 7200 sec. These plots are intended to be used for comparison with the next simulation run. Figure 2.5.1a shows the in-plane and out-of-plane angles which are almost unaffected by the damping provided by the longitudinal dampers, as can be seen more clearly in Figures 2.5.1b and c. Figures 2.5.1d, e and f show the tether tensions of tethers no. 1, 2 and 3 respectively, while Figures 2.5.1g, h

and i show the length variations of the associated longitudinal dampers. Figures 2.5.1j and k depict the in-plane (ϵ_1) and out-of-plane (ϵ_0) components of the lateral deflections respectively, while Figure 2.5.1l shows the moduli of the lateral deflections. Figures 2.5.1m and n show the phase-plane $\epsilon_1-\dot{\epsilon}_1$ and $\epsilon_2-\dot{\epsilon}_2$. The inward spiralling shown in Figure 2.5.1m is not due to damping but is the result of a beating phenomenon. The tether tensions are shown in Figures 2.5.1p, q and r for tethers no. 1, 2 and 3 respectively. Figure 2.5.1s shows the components of the acceleration on board the Space Station: ACH is the flight-direction, ACL the transverse and ACV the vertical component. The acceleration components at the variable-g laboratory are shown in Figures 2.5.1t, u and v respectively. Figure 2.5.1v clearly shows the steady state, vertical acceleration bias due to the 1 km offset of the variable-g laboratory from the system C.M. Figures 2.5.1w, x and y show the x,y and z components of the system C.M. referred to the orbiting reference frame. Because the initial conditions have non-zero total angular momentum, the x-component (flight-direction) of the C.M. drifts, while the y-component (transverse) and the z-component (vertical) oscillate. The system C.M. is following a slightly elliptic orbit and the orbital plane is also slightly oscillating. Figure 2.5.1z and Figure 2.5.1za show the side and front-view respectively of the system at intervals of 40 sec for 7200 sec. The scale of the abscissa is largely expanded in order to show the various oscillatory modes. Since mass no. 1, the balancing mass, is shown at the top of the figures, the Earth is on the side of the positive ordinates.

The fourth simulation has been run for 10,000 sec with the same initial conditions of simulation no. 3. This time the in-plane librational and lateral damping algorithms are activated in order to damp out the relevant oscillatory modes. Figures 2.5.2a-za show the results of the simulation. Each figure must be compared to the equivalent figure from the previous set of plots (Figures

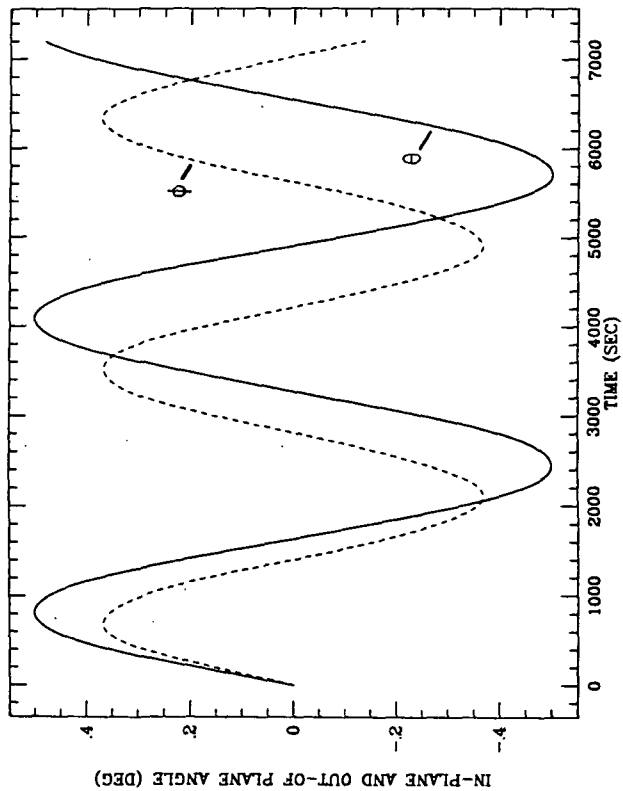


Figure 2.5.1a

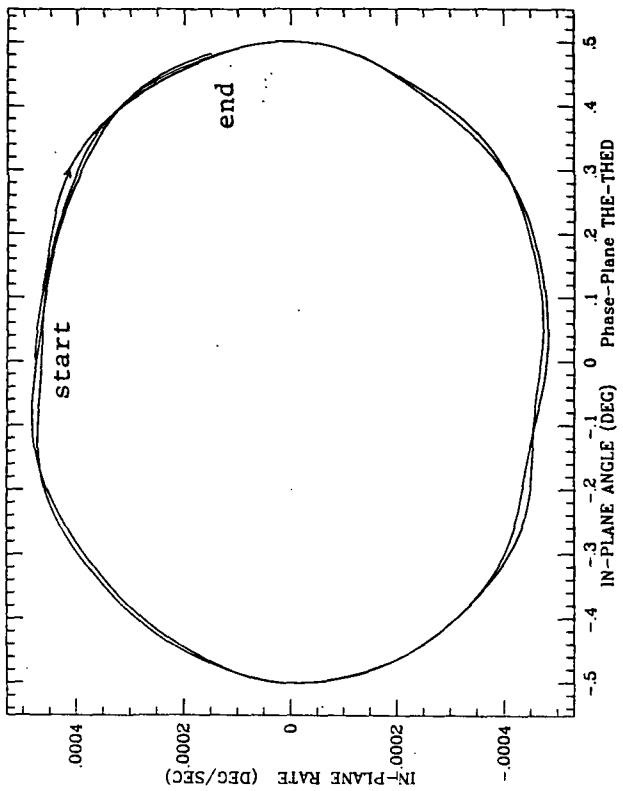


Figure 2.5.1b

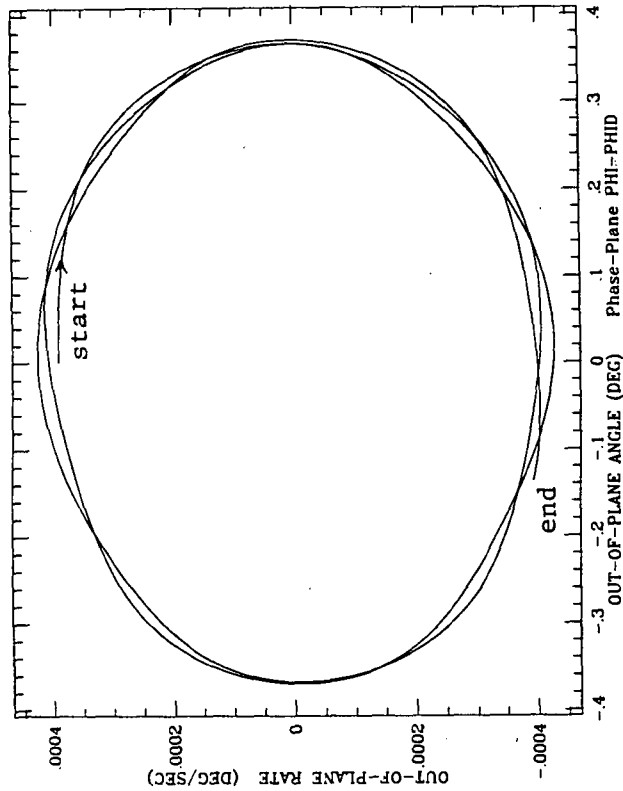


Figure 2.5.1c

ORIGINAL PAGE IS
OF POOR QUALITY

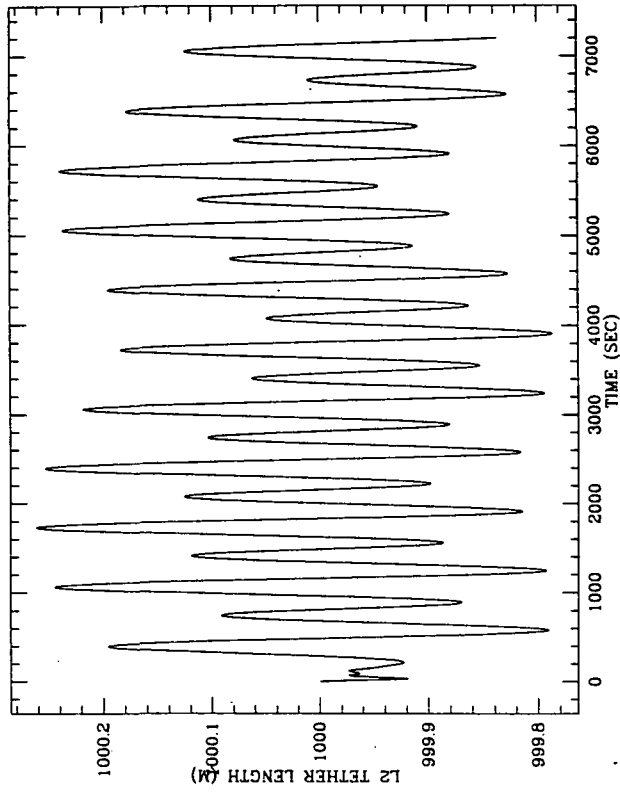


Figure 2.5.1e

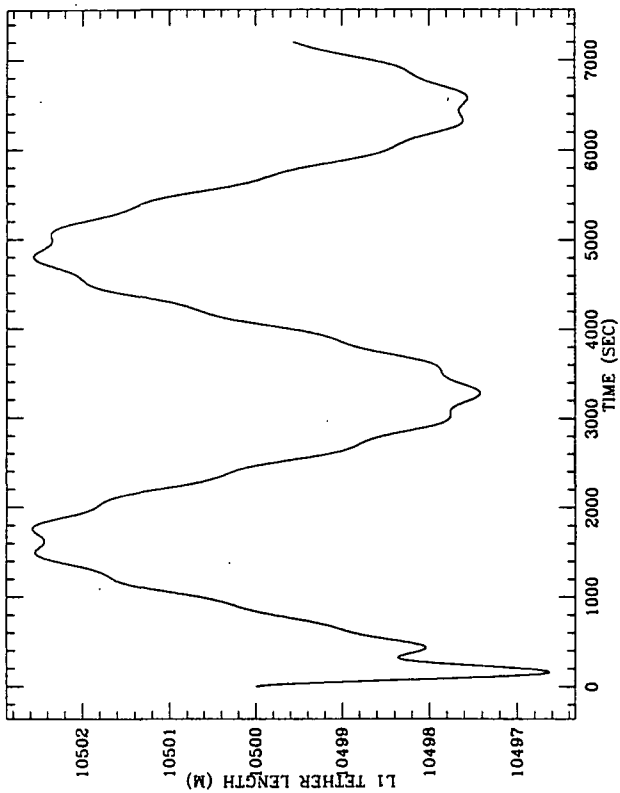


Figure 2.5.1d

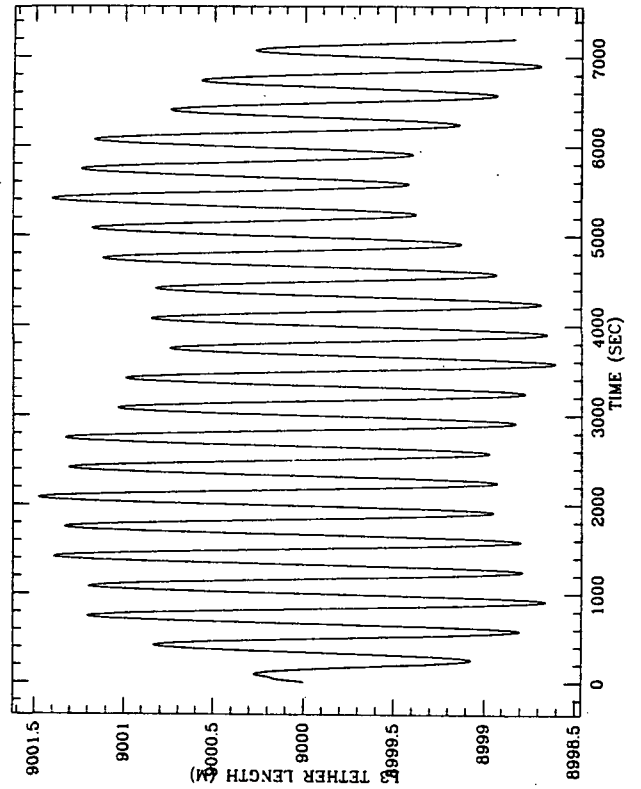


Figure 2.5.1f

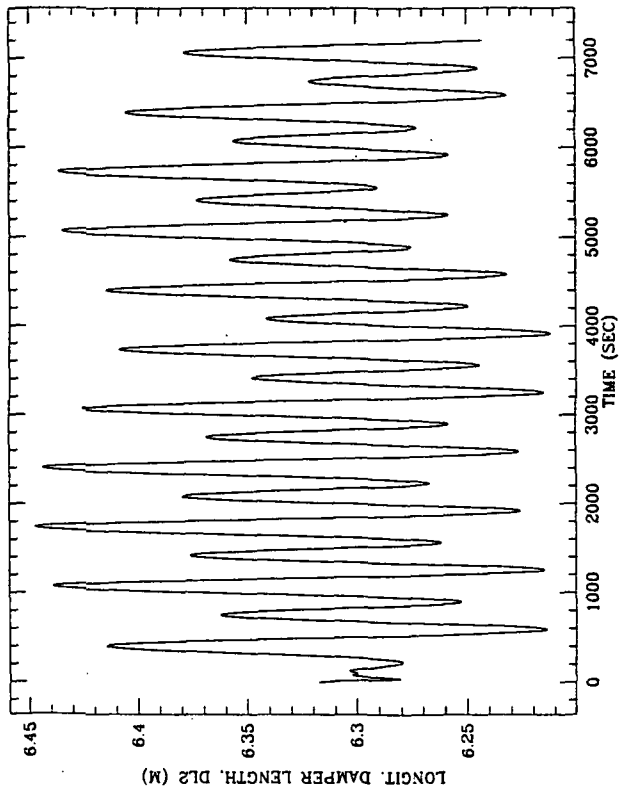


Figure 2.5.1h

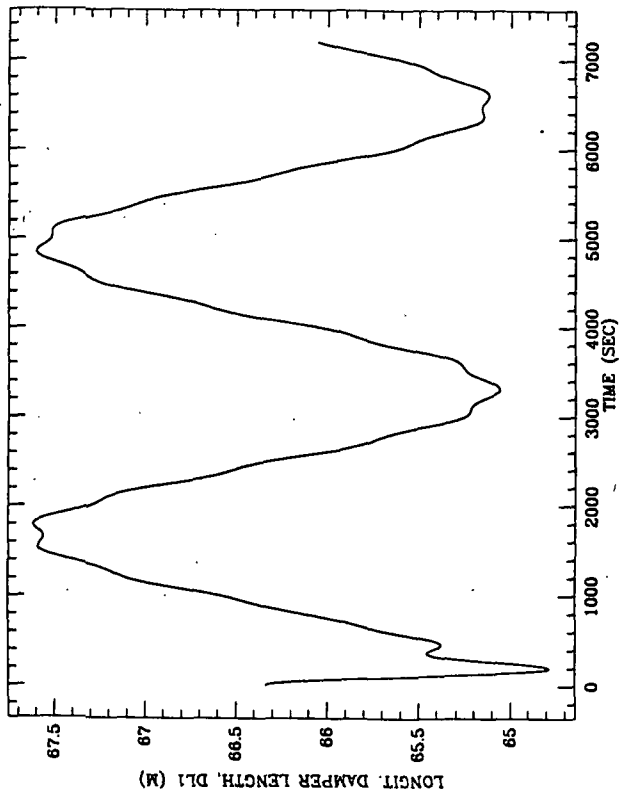


Figure 2.5.1g

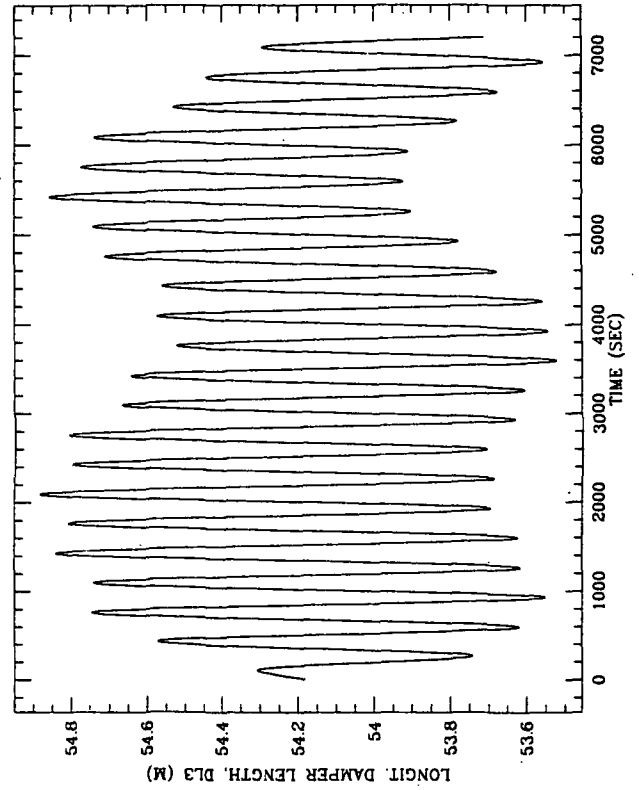


Figure 2.5.1i

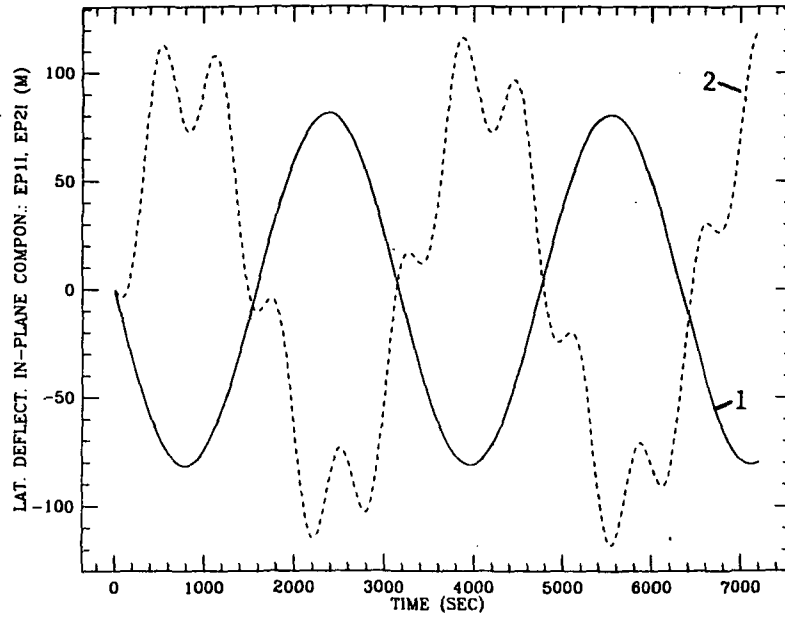


Figure 2.5.1j

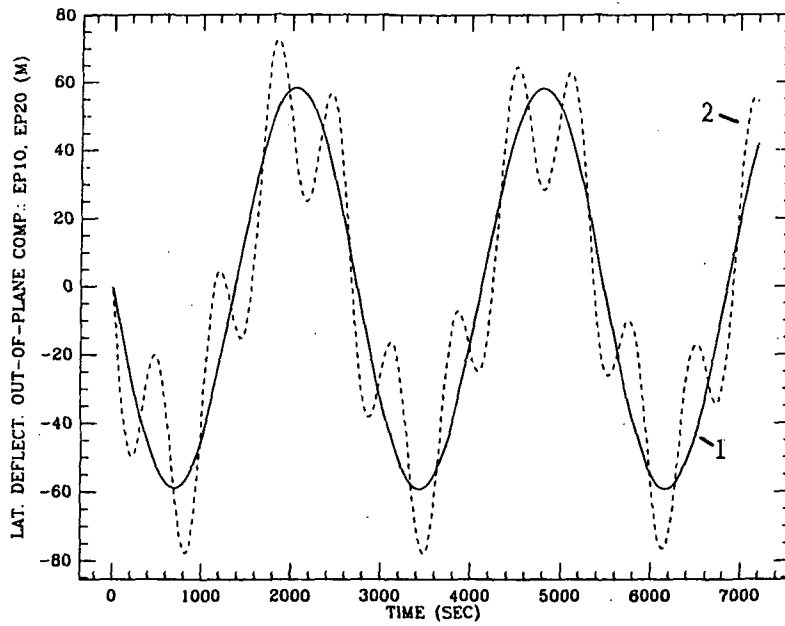


Figure 2.5.1k

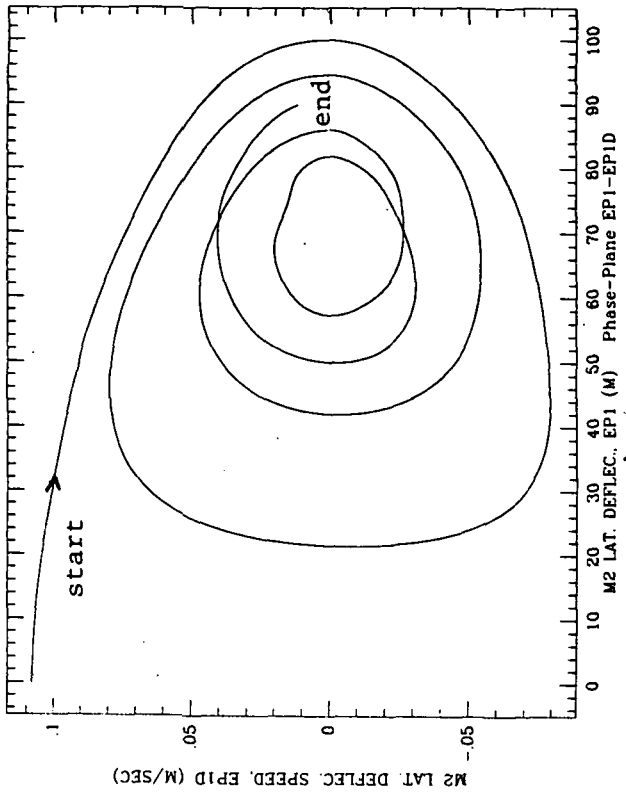


Figure 2.5.1m

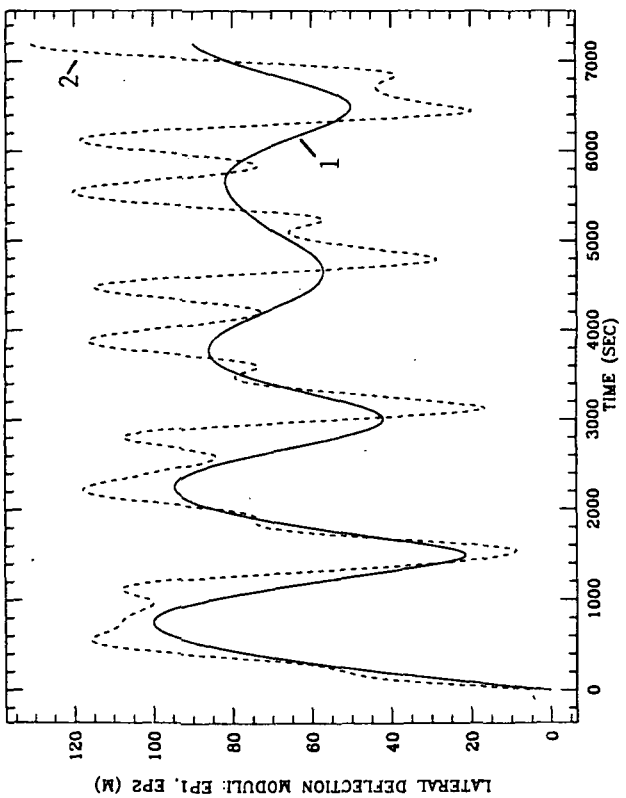


Figure 2.5.1l

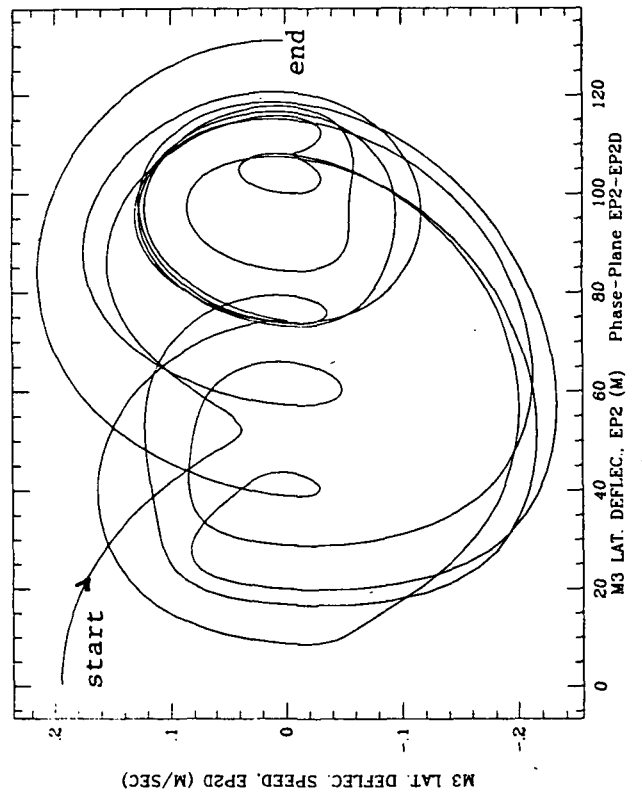


Figure 2.5.1n

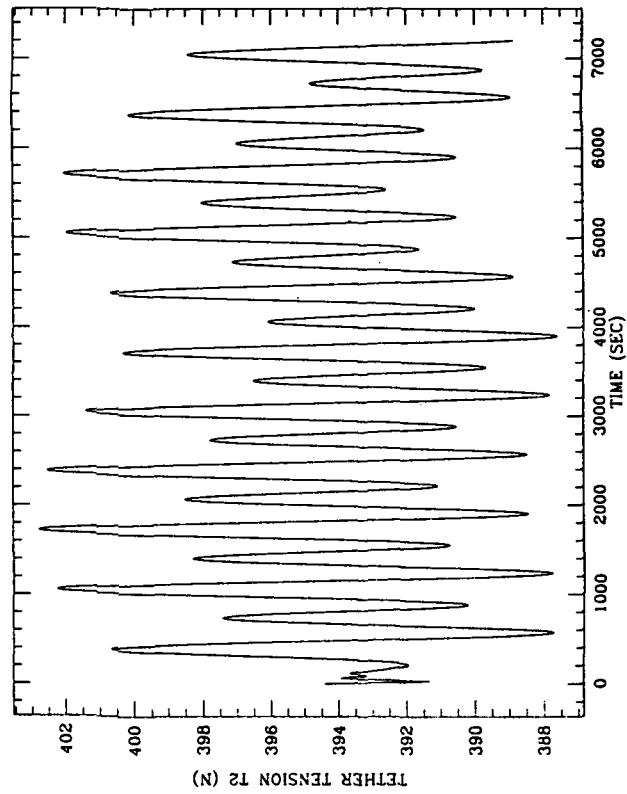


Figure 2.5.1q

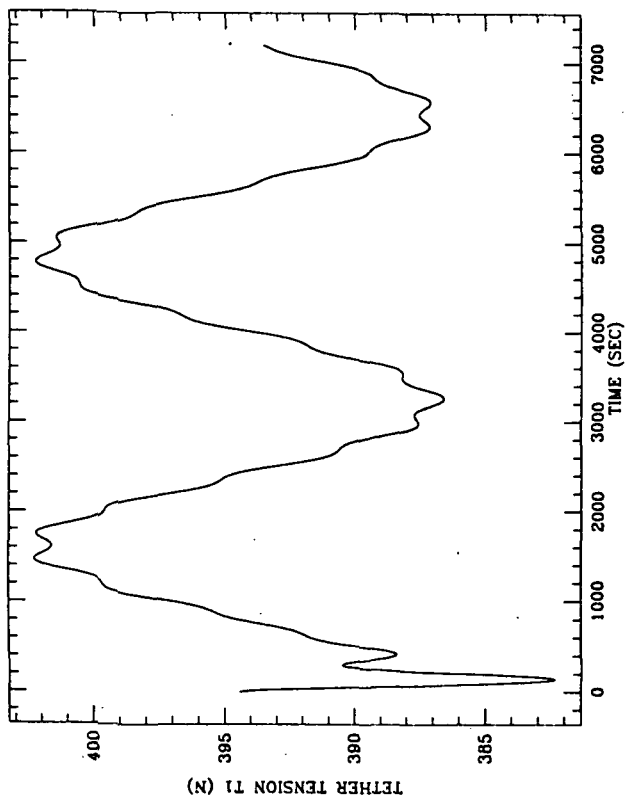


Figure 2.5.1p

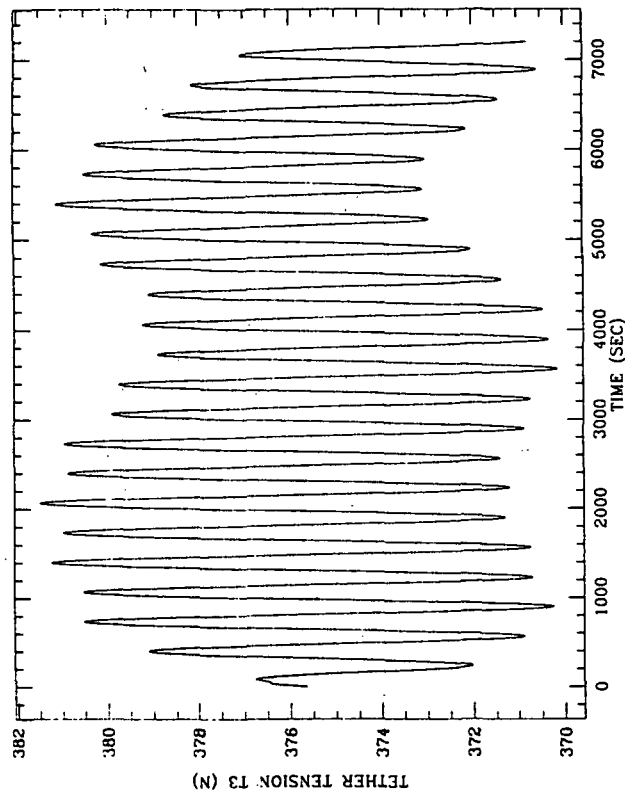


Figure 2.5.1r

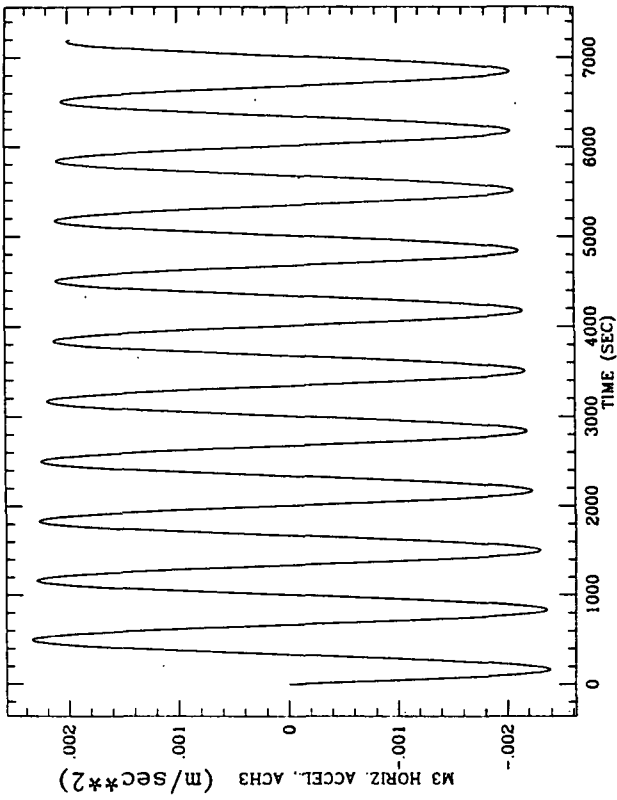


Figure 2.5.lt

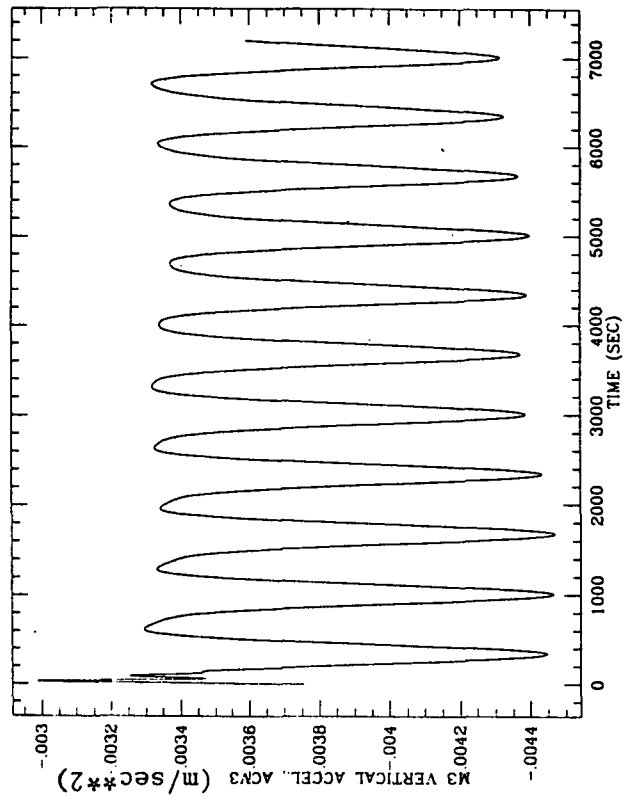


Figure 2.5.lv

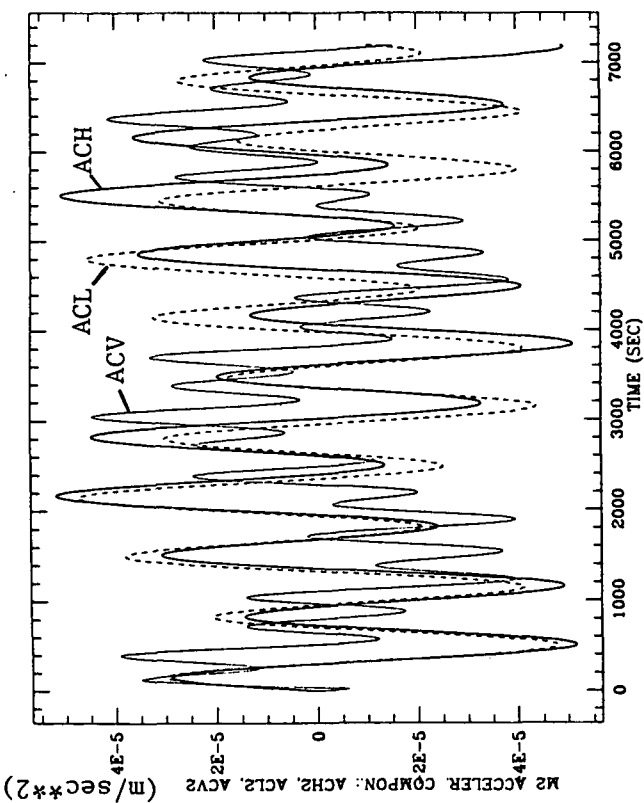


Figure 2.5.ls

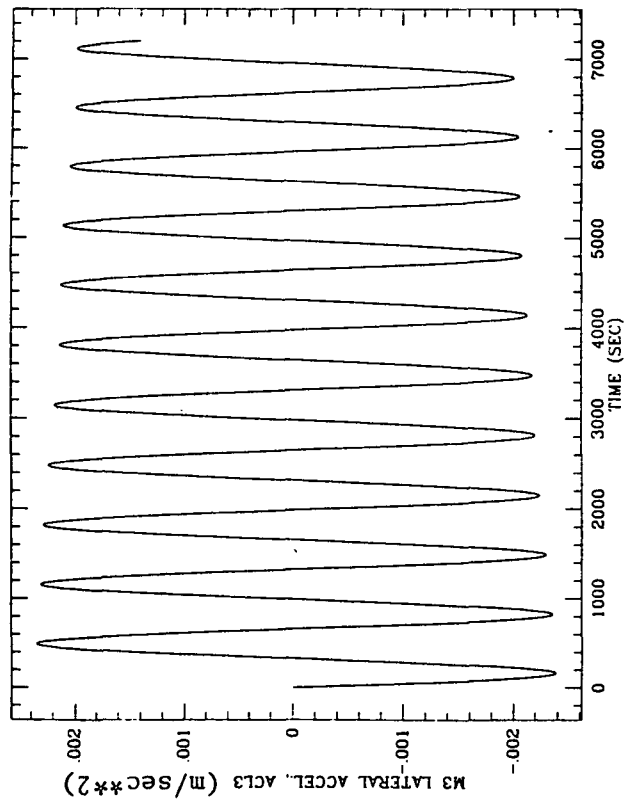


Figure 2.5.lu

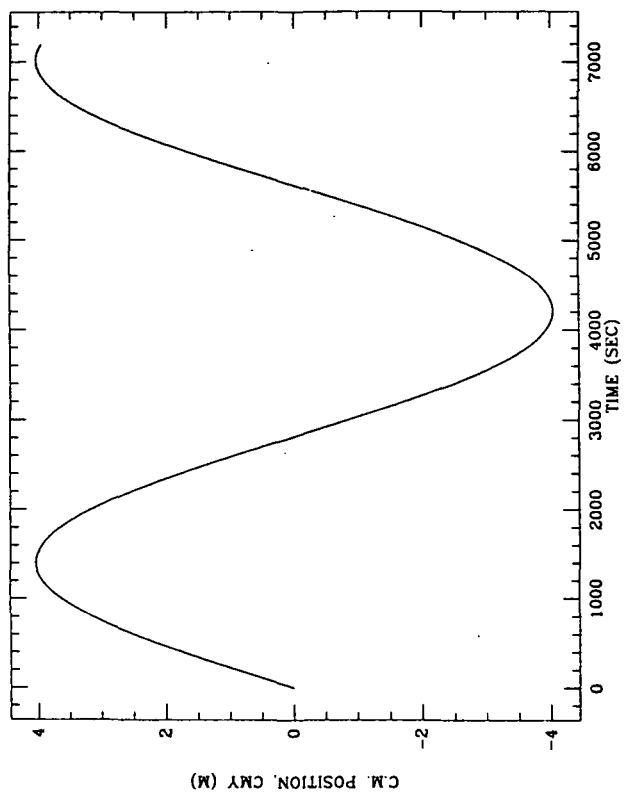


Figure 2.5.1x

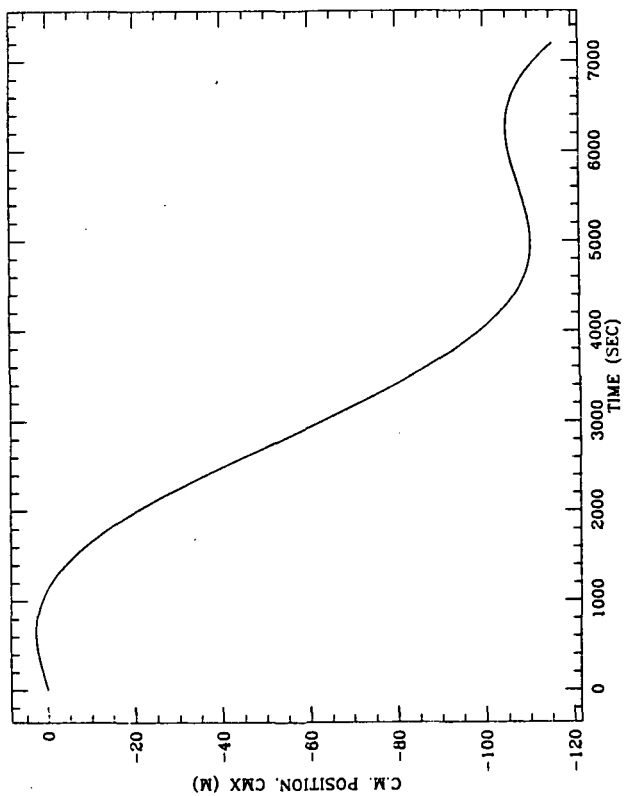


Figure 2.5.1w

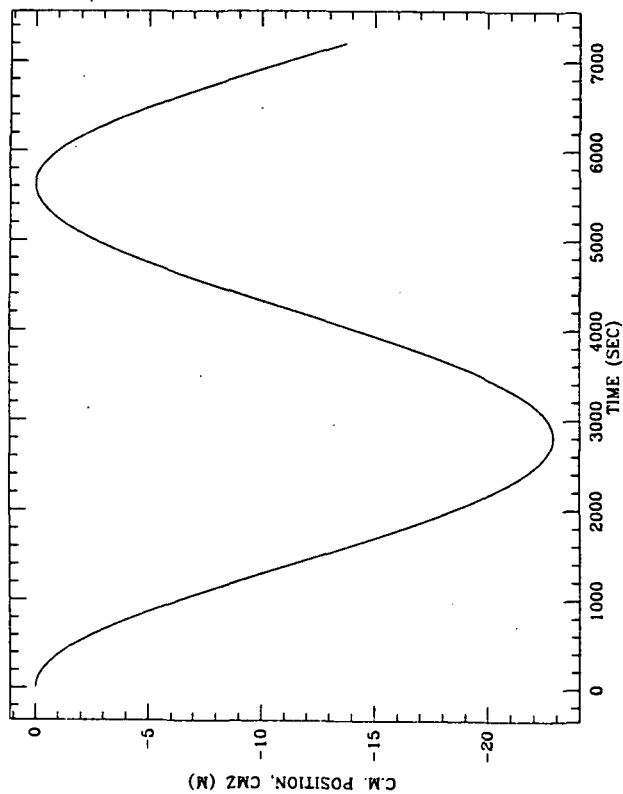


Figure 2.5.1y

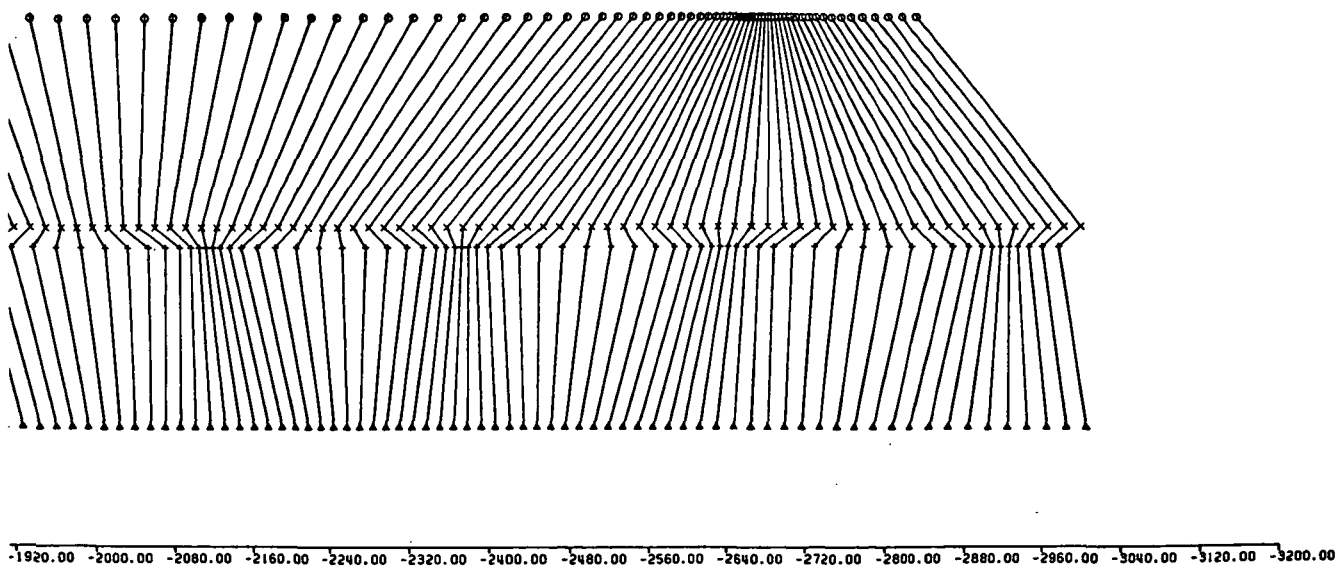
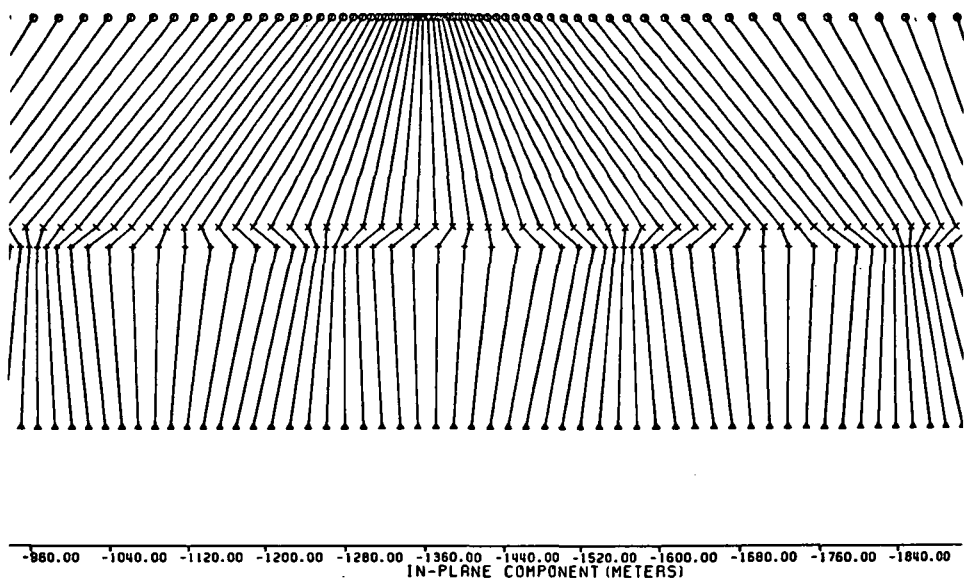
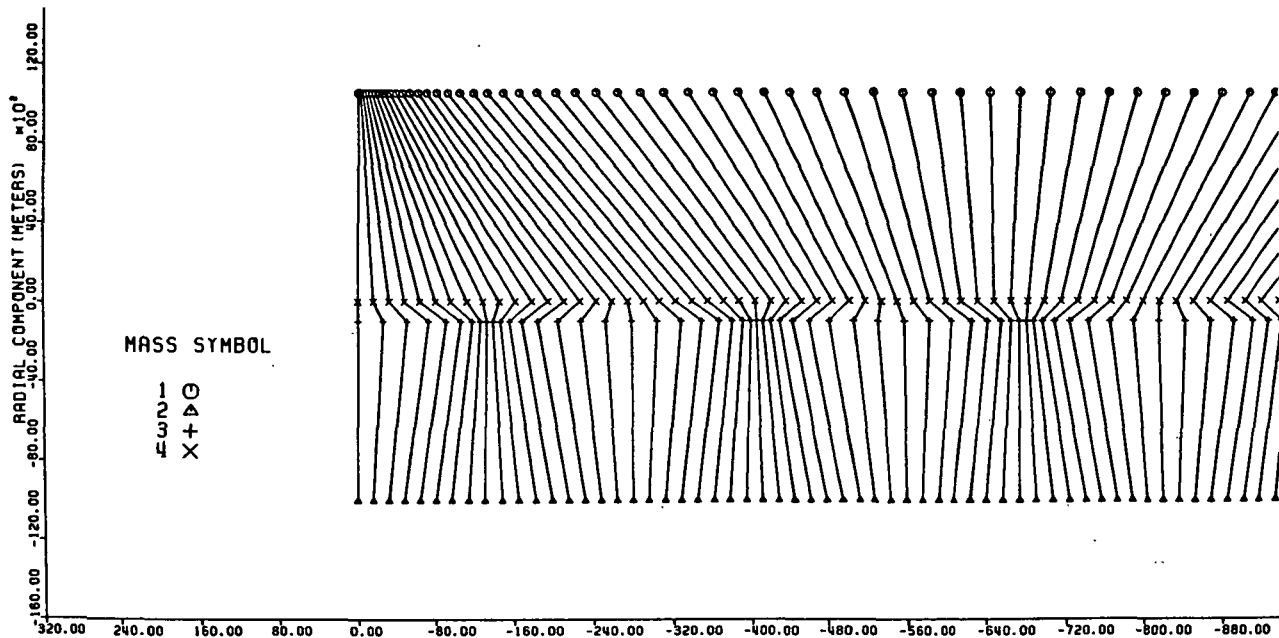


Figure 2.5.1z - Expanded Scale, Side-View Plotted Every 40 Sec for 7200 Sec. Longitudinal Dampers On.

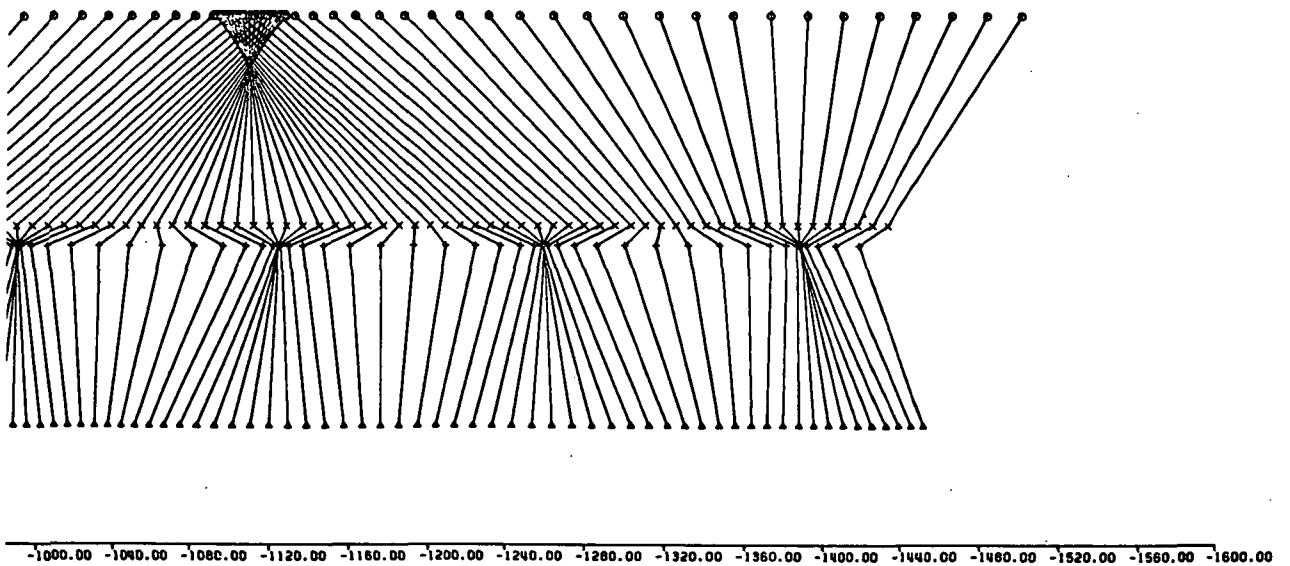
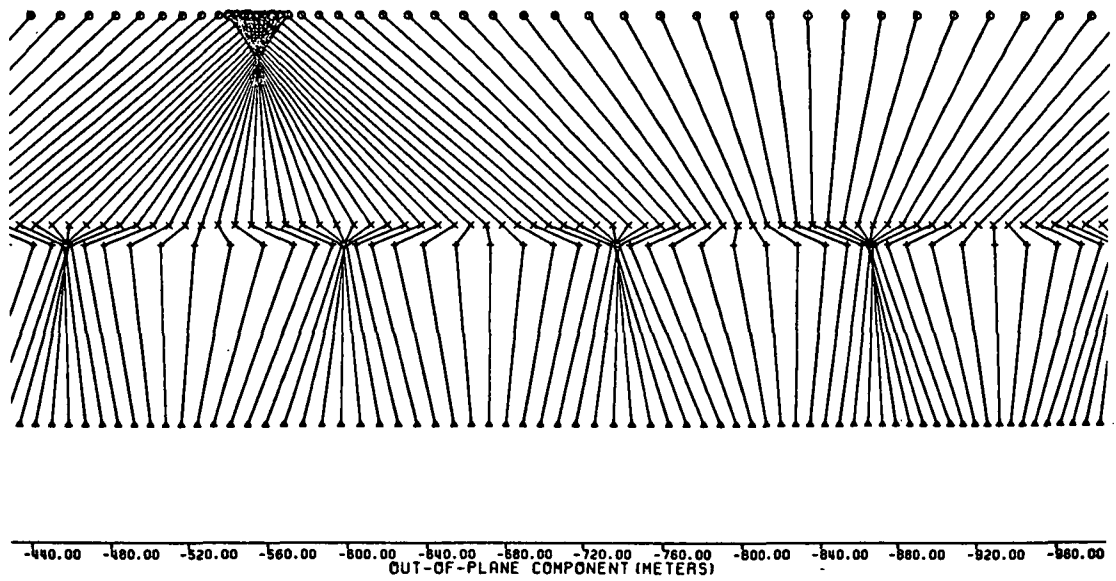
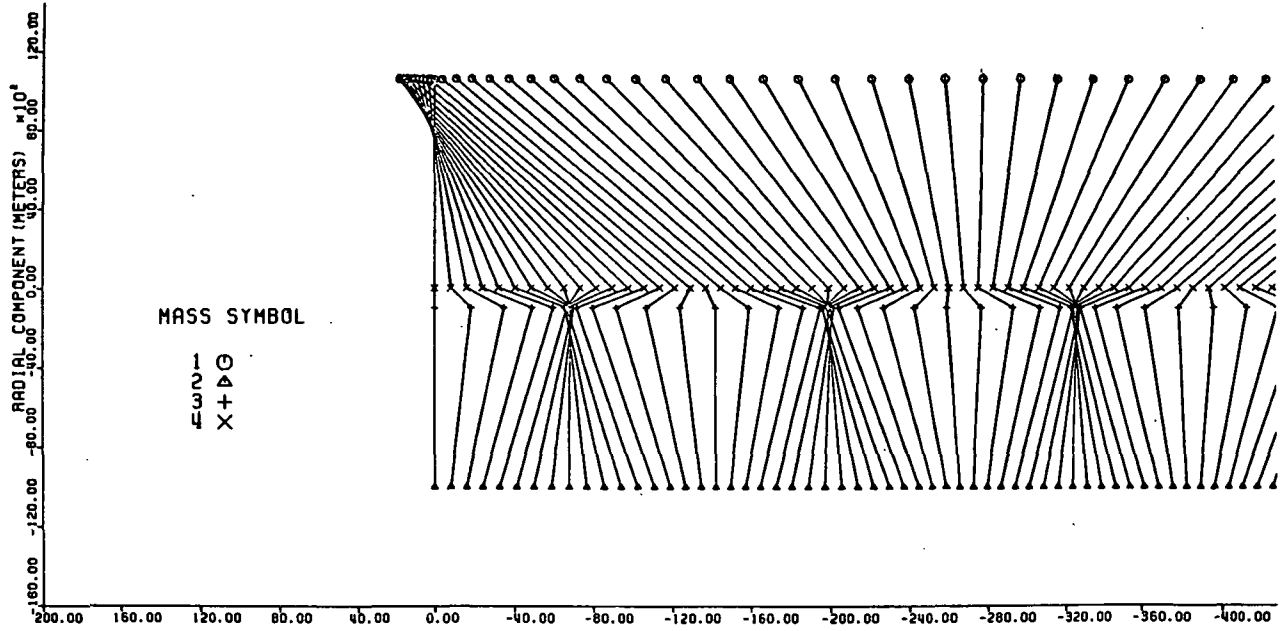


Figure 2.5.1za - Expanded Scale, Front-View Plotted Every 40 Sec for 7200 Sec. Longitudinal Dampers On.

2.5.1a-za). The activation of the in-plane librational and lateral dampers damp out effectively the in-plane libration and the in-plane components of the lateral oscillatory modes as may be easily seen throughout the set of plots. The out-of-plane dynamics are, on the contrary, negligibly affected by the dampers. The out-of-plane dynamics are therefore responsible for the residual oscillations of the system both directly and through couplings. Figures 2.5.2m and n, for example, show the phase-planes $\epsilon_1-\dot{\epsilon}_1$ and $\epsilon_2-\dot{\epsilon}_2$. The limit cycles in these figures are due to the out-of-plane dynamics. Since the derivatives $\dot{\epsilon}_1$ and $\dot{\epsilon}_2$ change sign when $\epsilon_1 = 0$ or $\epsilon_2 = 0$ respectively, the two phase-planes have an unusual shape due to the discontinuities of the derivatives at the zero crossing. The net result of the dampers can be seen in Figure 2.5.2s and Figures 2.5.2t, u and v. The librational/lateral dampers (at least with the current algorithms) initially produce higher acceleration levels at the Space Station, but after 10,000 sec the vertical (ACV) and flight-direction (ACH) components are strongly reduced. The transverse component (ACL) depends upon the out-of-plane dynamics and is therefore negligibly affected by the current dampers. The initial increase in the acceleration level at the Station will be investigated more in the next reporting period with the aim of reducing such increase. The acceleration level at the variable-g laboratory (m_3) does not show any initial amplitude increase with respect to simulation no. 3. The flight-direction (Figure 2.5.2t) and the vertical component (Figure 2.5.2v) are effectively damped out at the end of the simulation; in particular the vertical component reaches the steady state value consistent with the 1 km offset from the system C.M. Figures 2.5.2z and za show the side-view and the front-view of the system with longitudinal and librational/lateral dampers switched on. The shape of the constellation is plotted every 40 sec for 7200 sec. These two plots must be compared to Figures 2.5.1z and za respectively; the dramatic effect of the

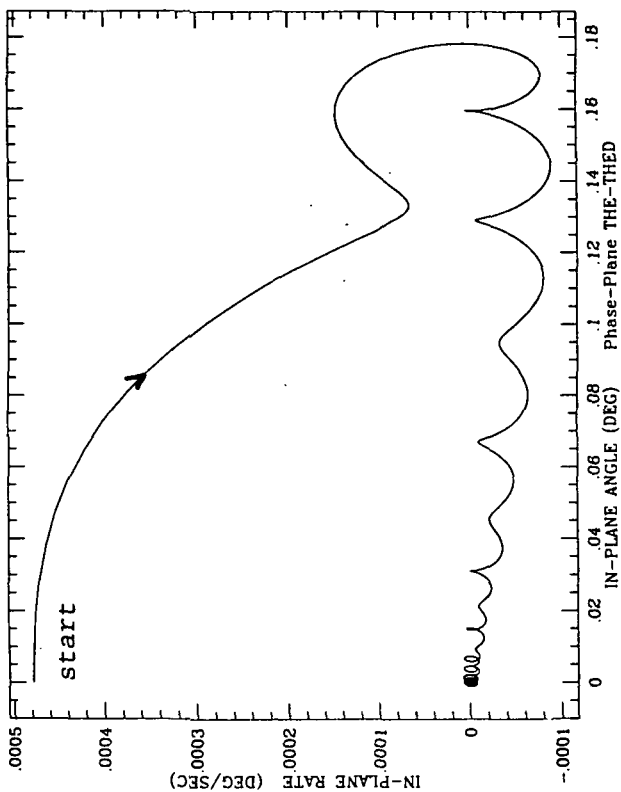


Figure 2.5.2b

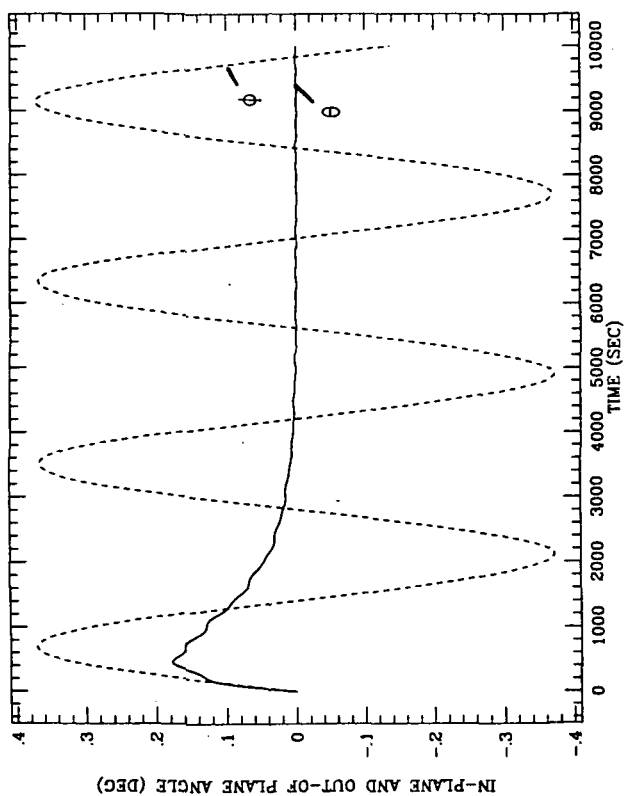


Figure 2.5.2a

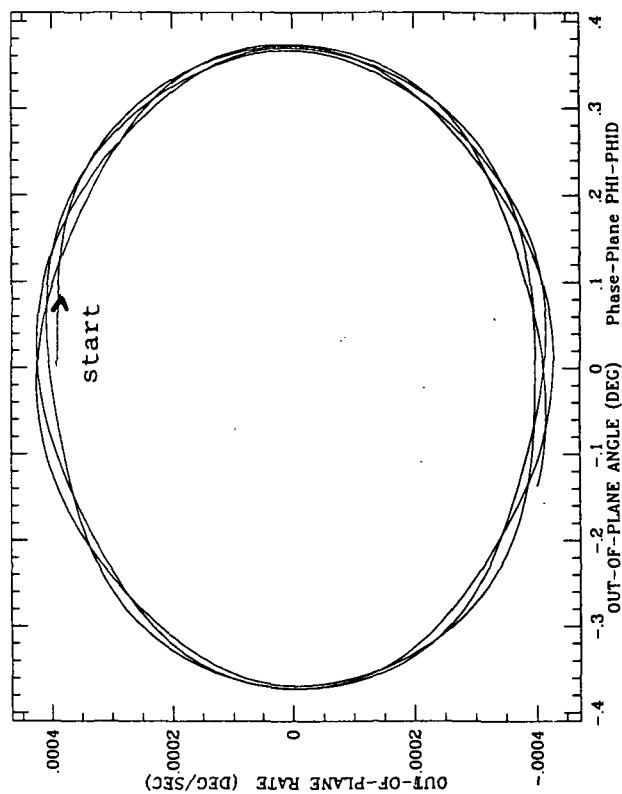


Figure 2.5.2c

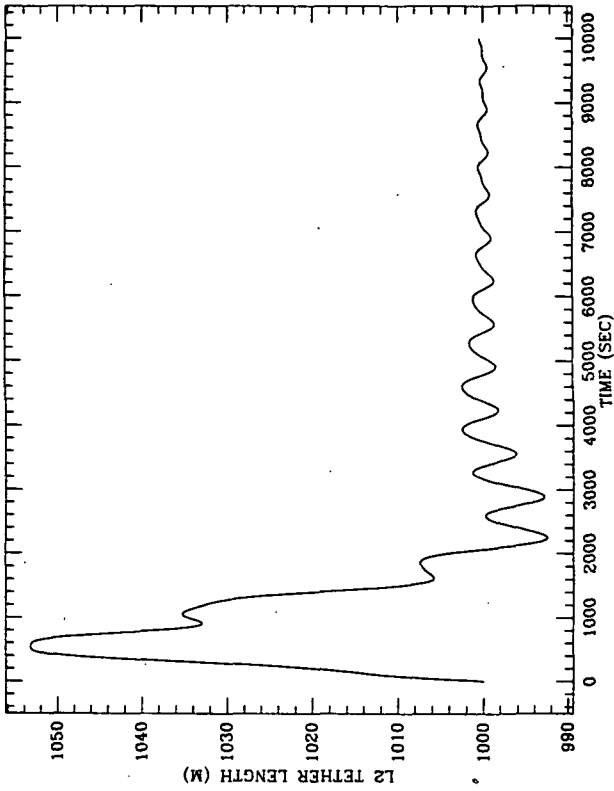


Figure 2.5.2e

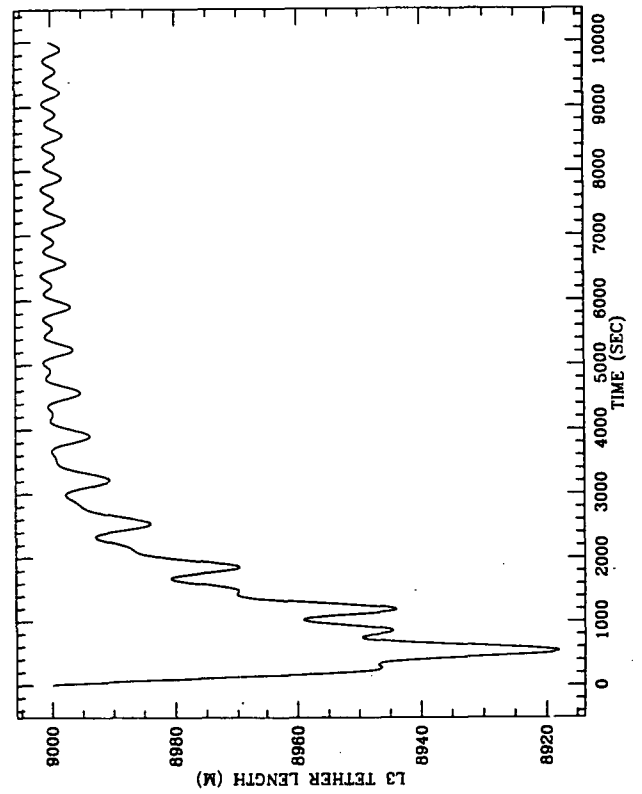


Figure 2.5.2f

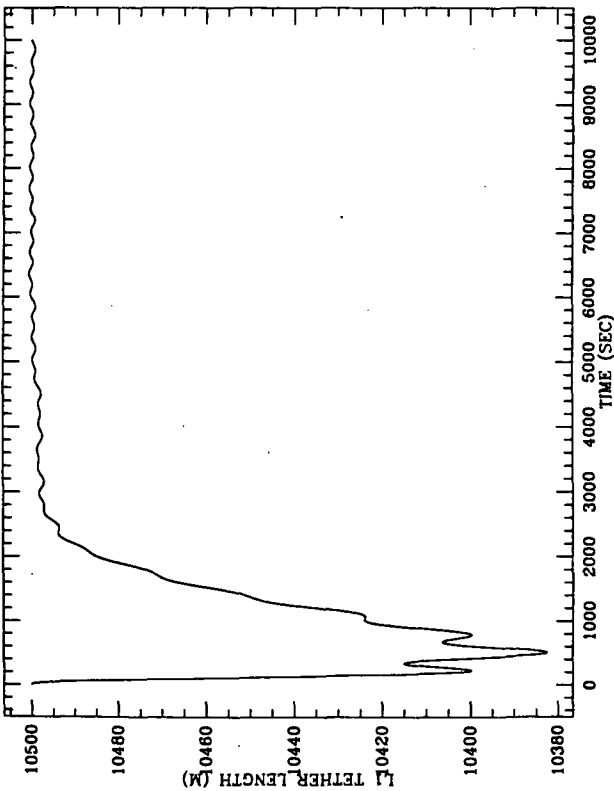


Figure 2.5.2d

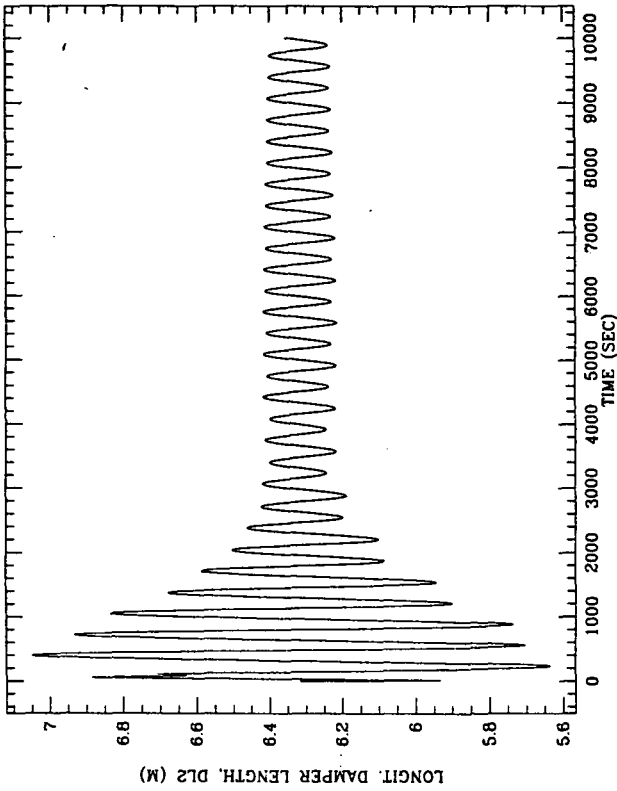


Figure 2.5.2h

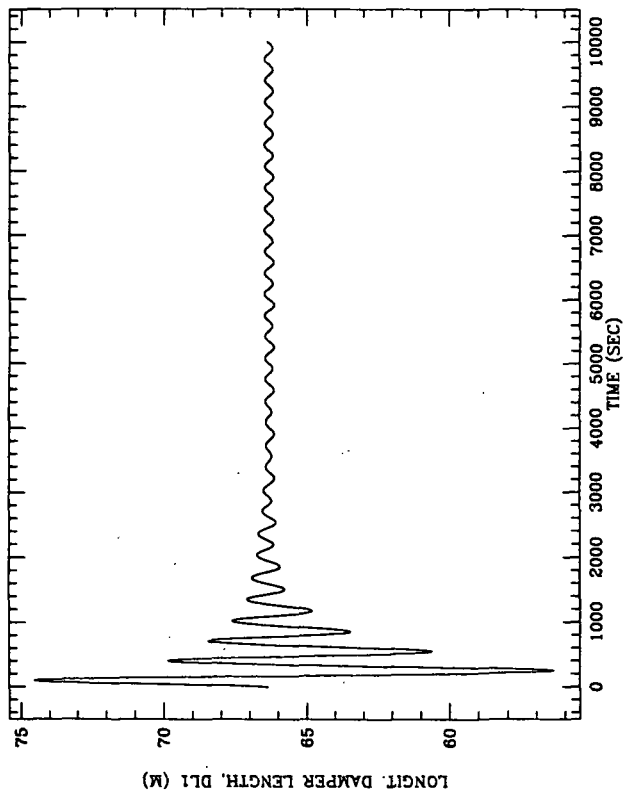


Figure 2.5.2g

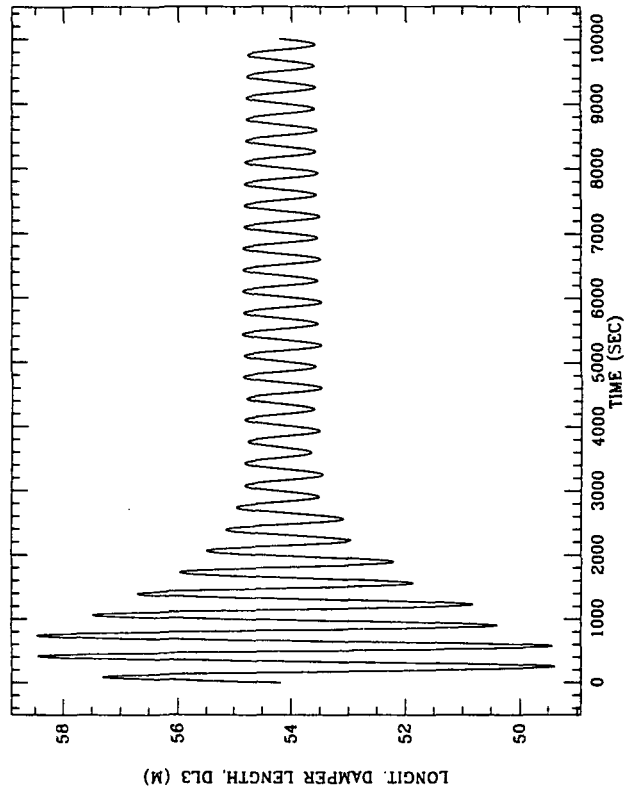


Figure 2.5.2i

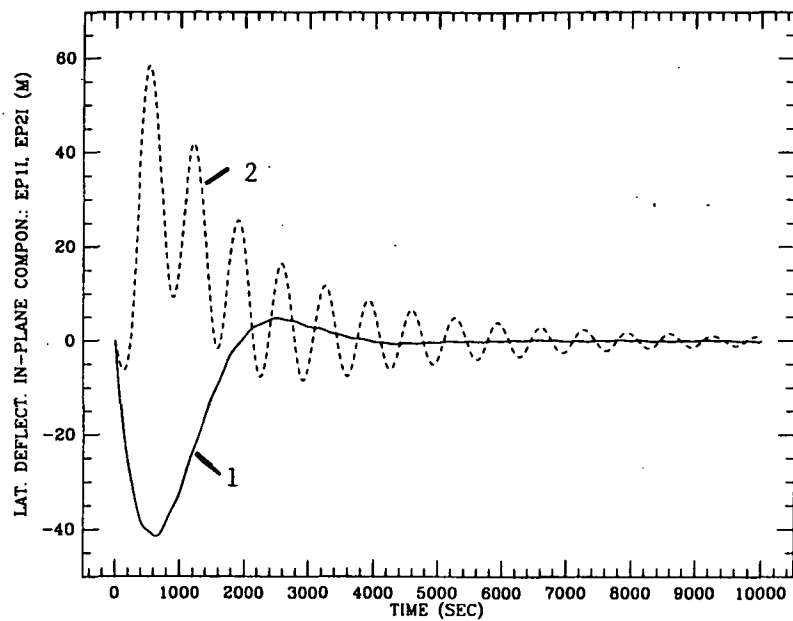


Figure 2.5.2j

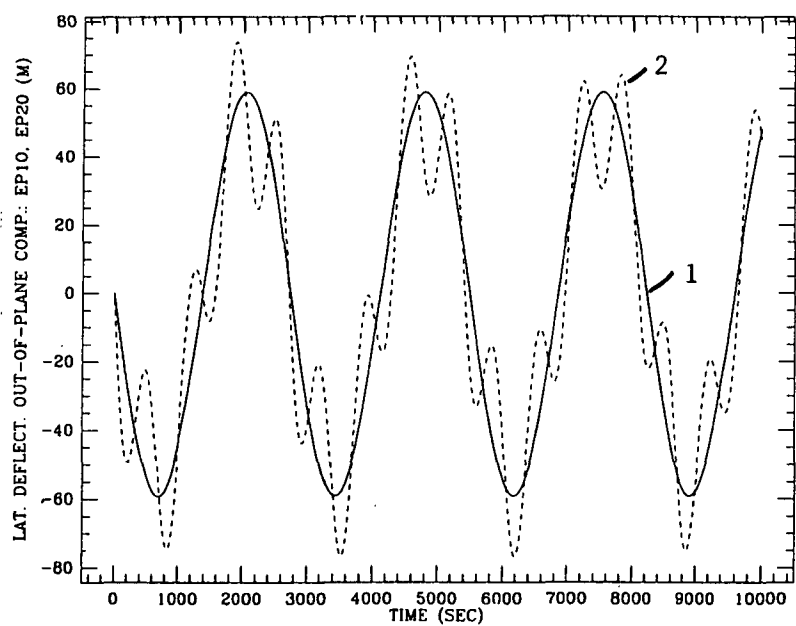


Figure 2.5.2k

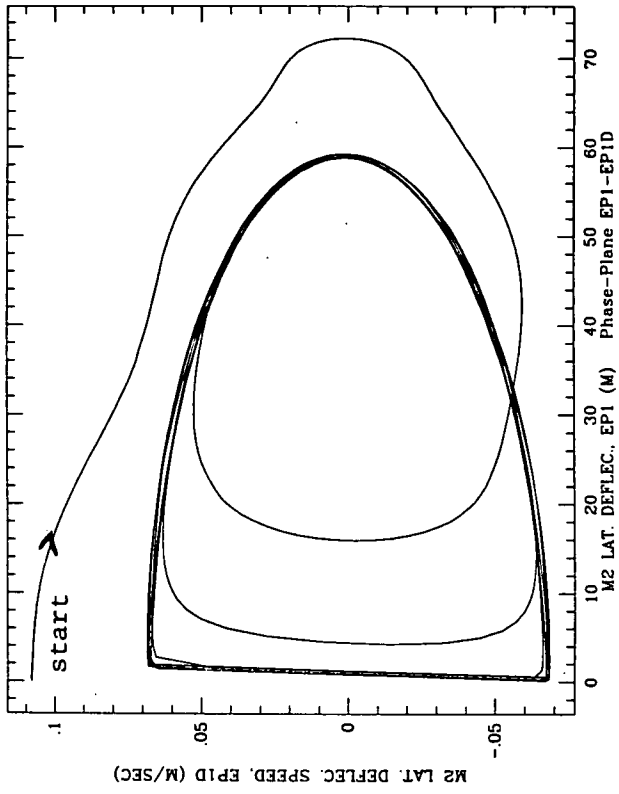


Figure 2.5.2m

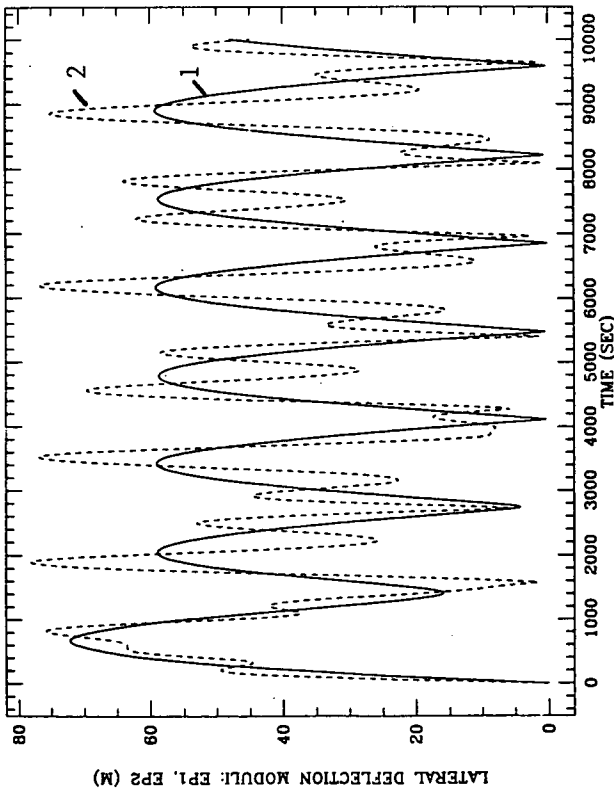


Figure 2.5.2l

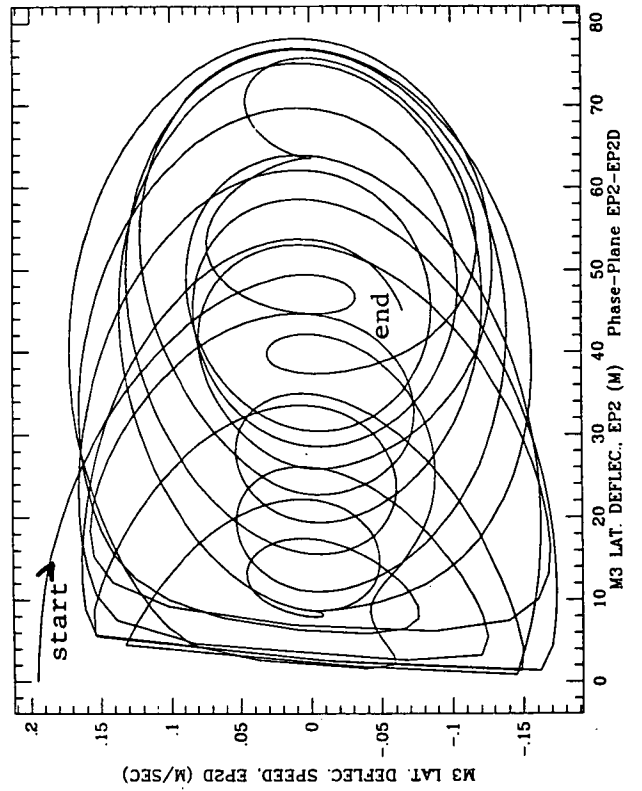


Figure 2.5.2n

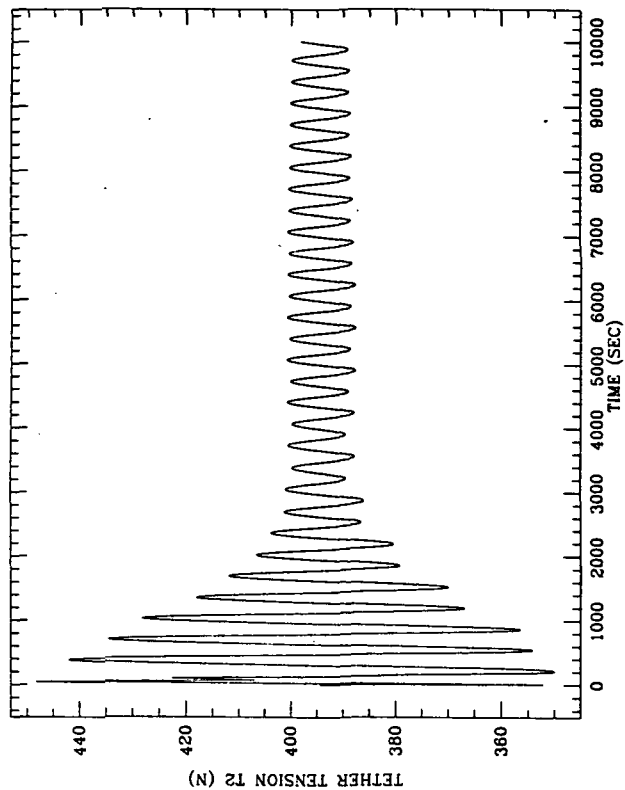


Figure 2.5.2q

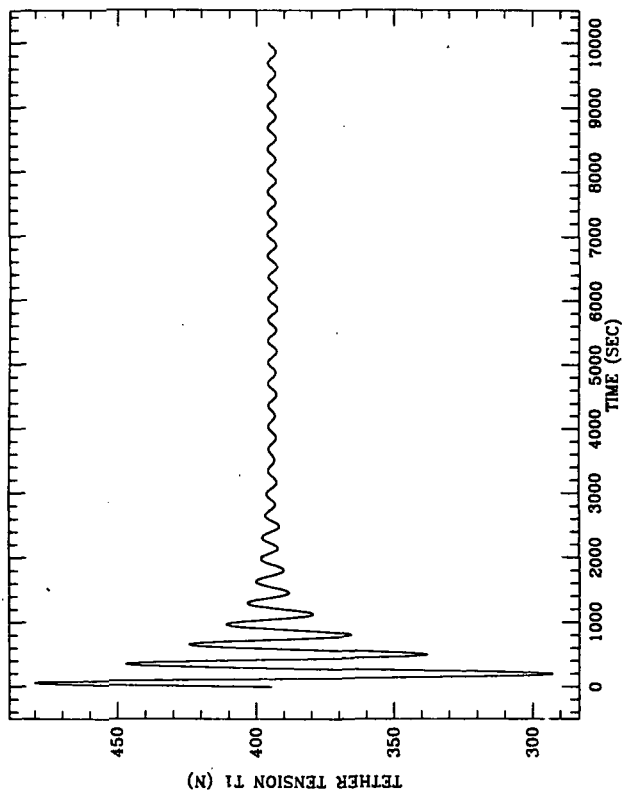


Figure 2.5.2p

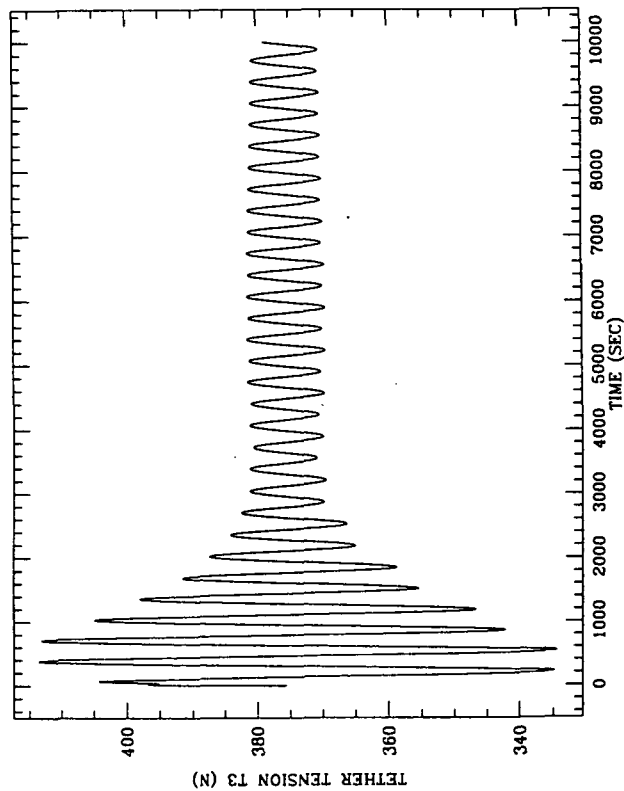


Figure 2.5.2r

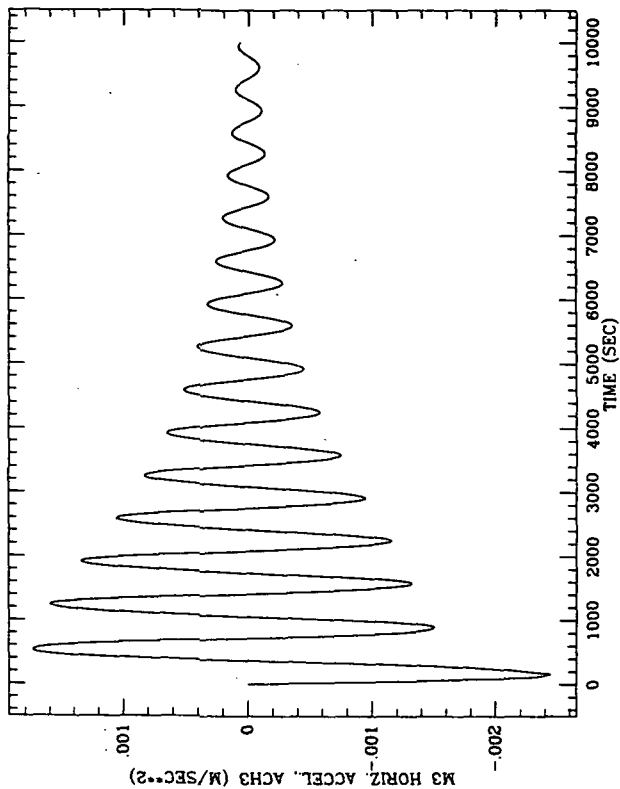


Figure 2.5.2t

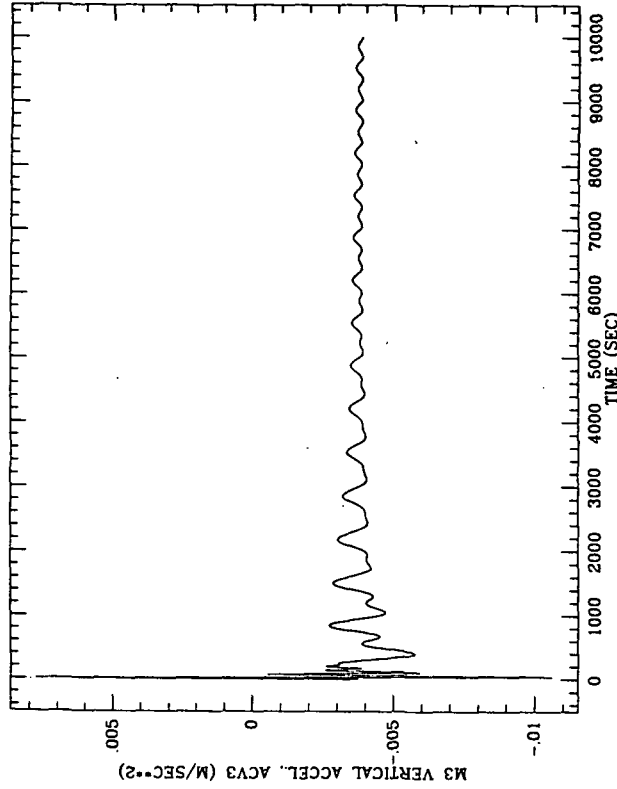


Figure 2.5.2v

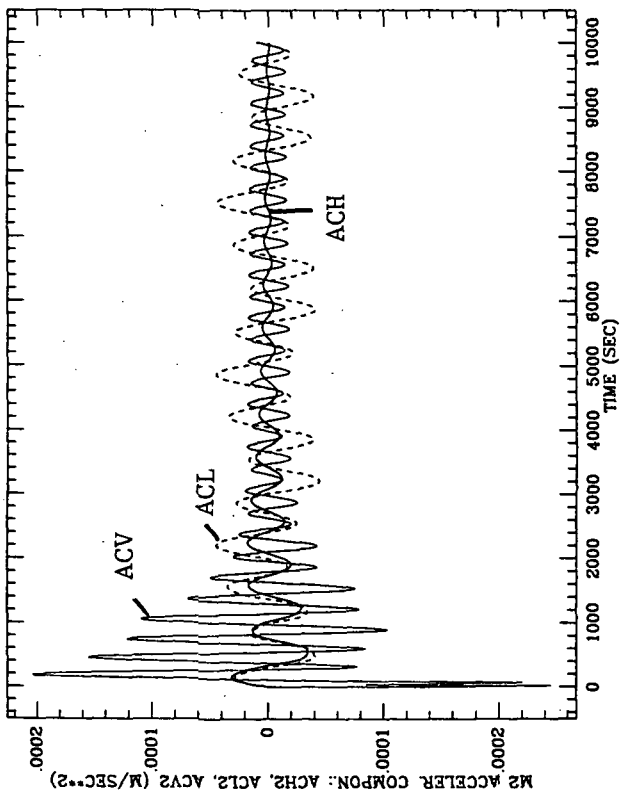


Figure 2.5.2s

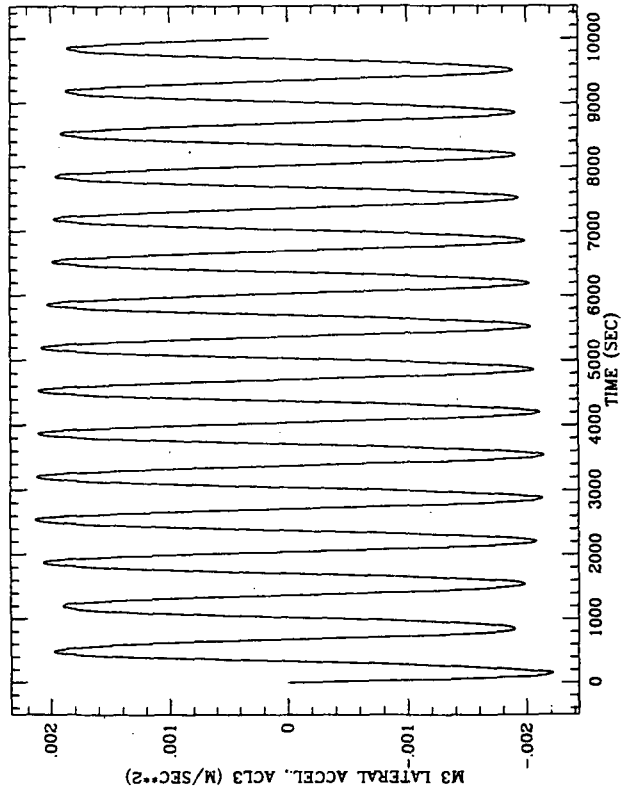


Figure 2.5.2u

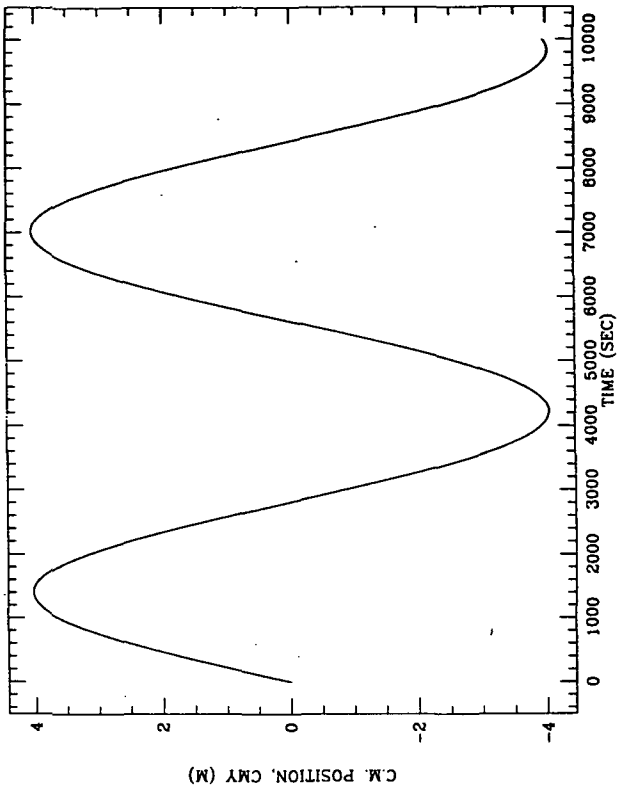


Figure 2.5.2x

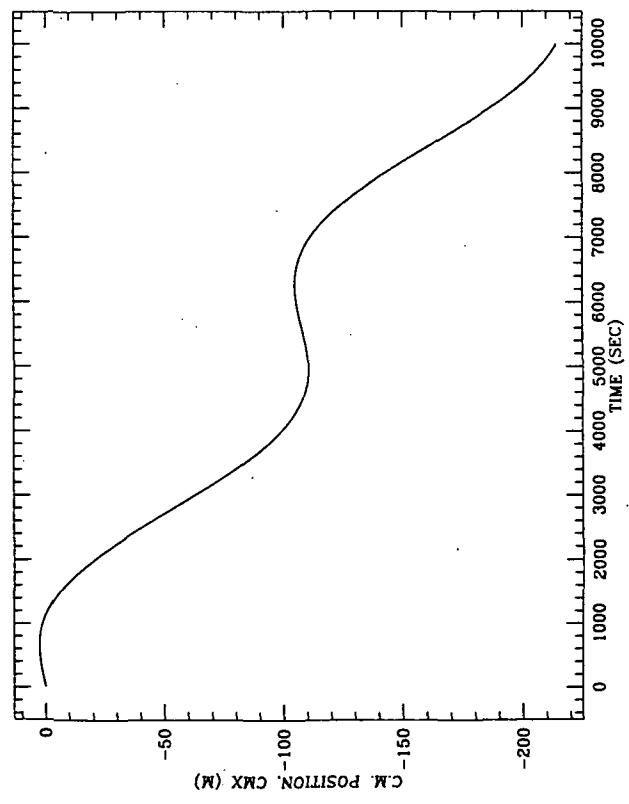


Figure 2.5.2w

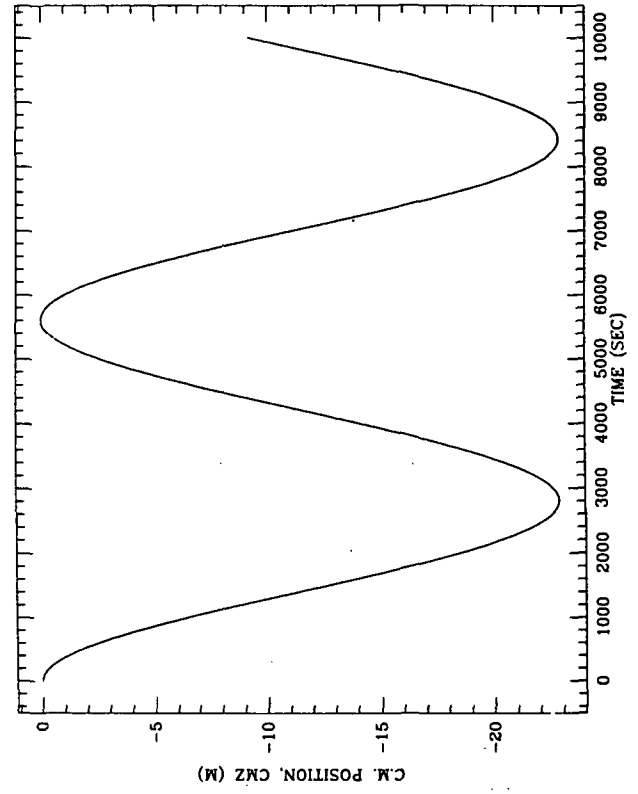


Figure 2.5.2y

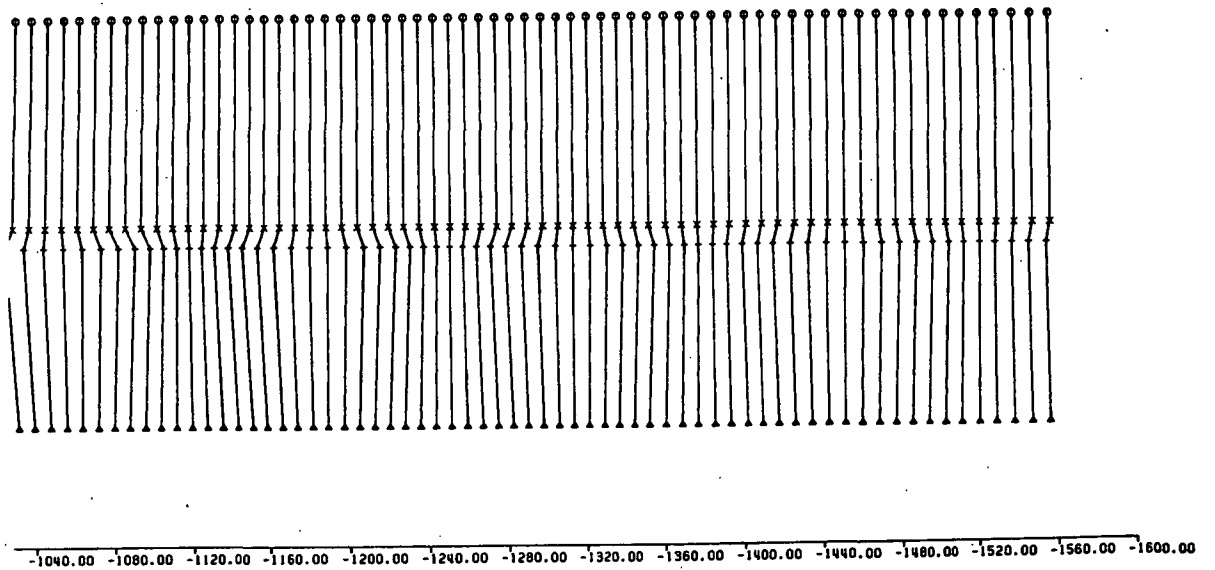
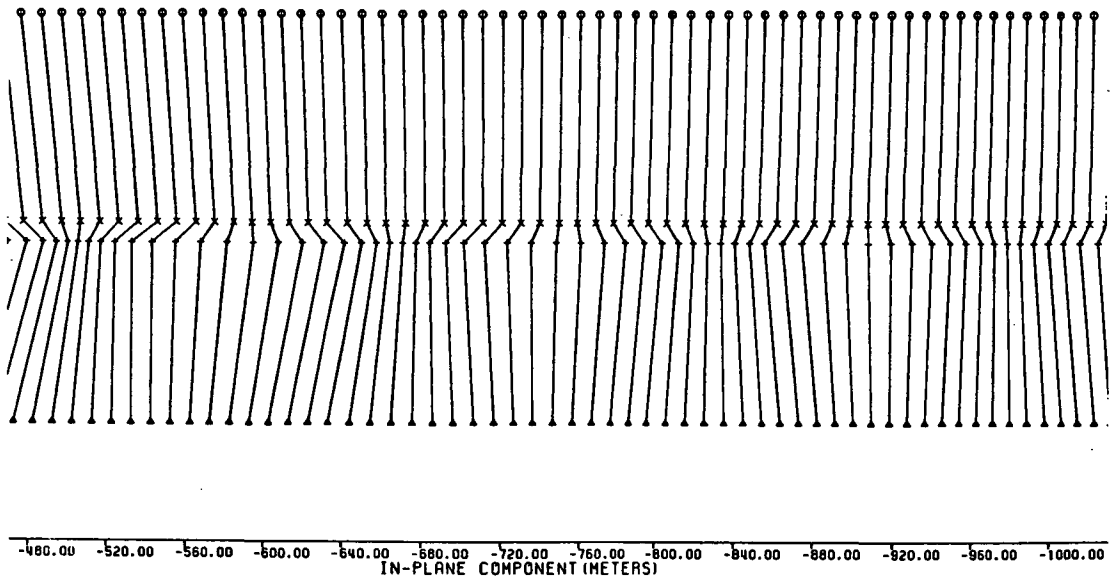
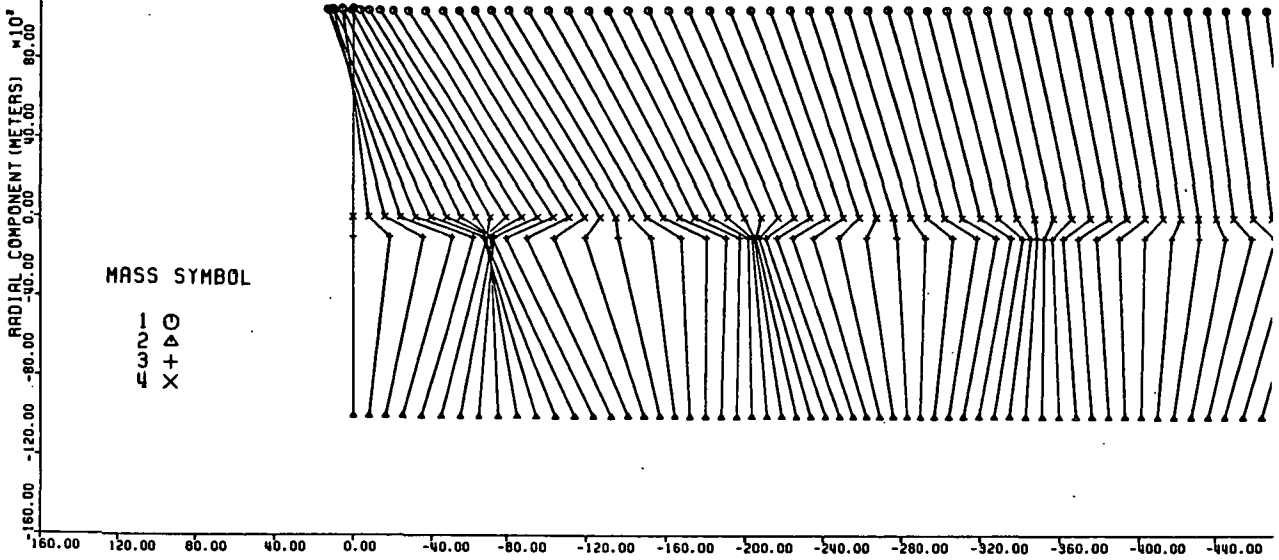


Figure 2.5.2z - Expanded Scale, Side-View Plotted Every 40 Sec for 7200 Sec.
Longitudinal + In-Plane Librational/Lateral Dampers On.

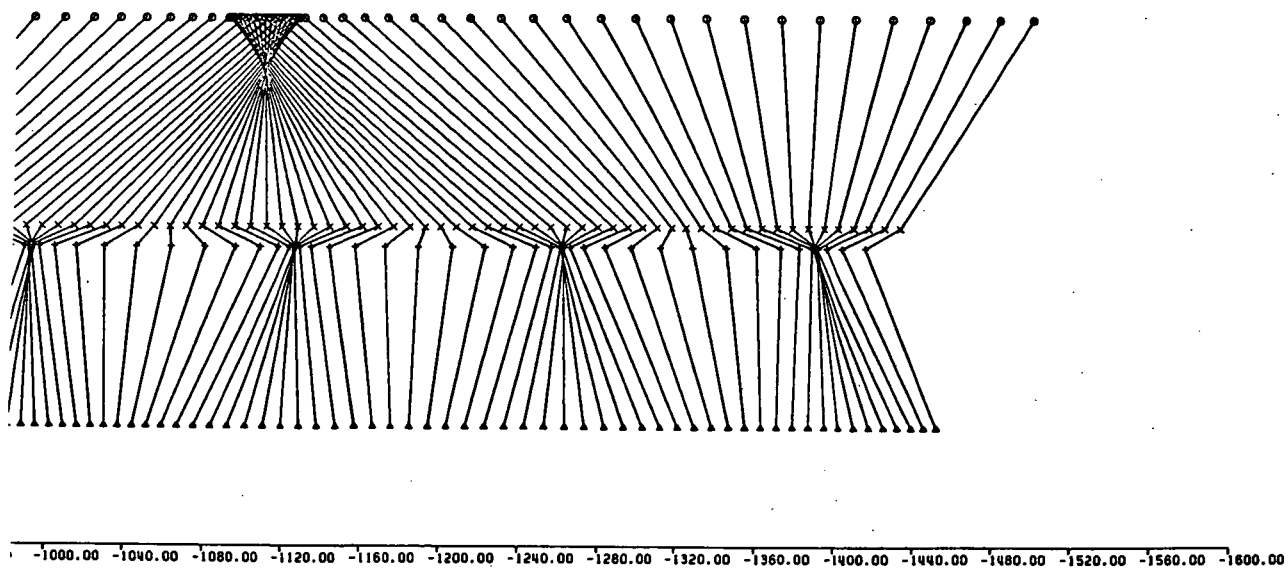
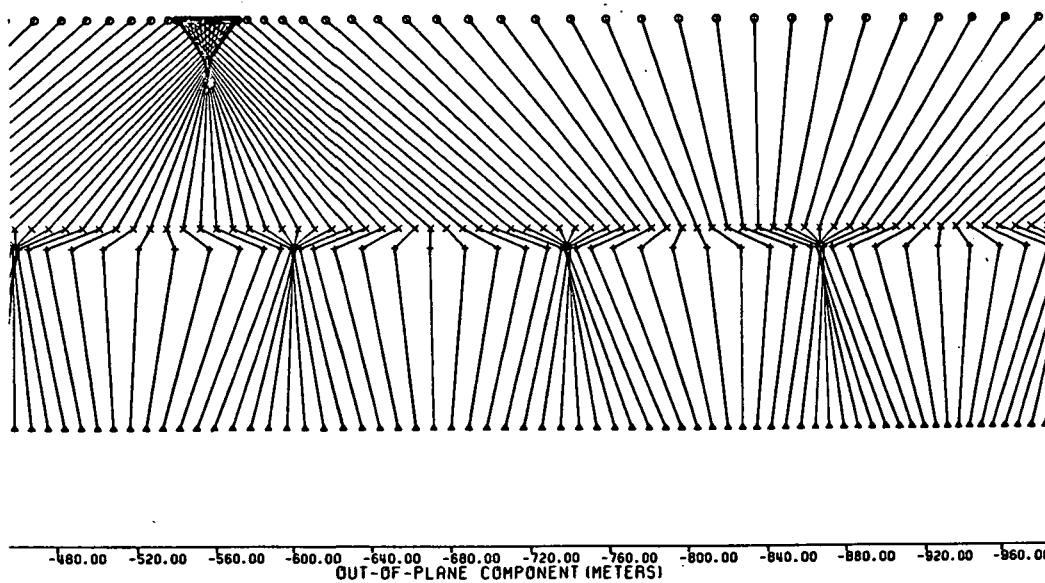
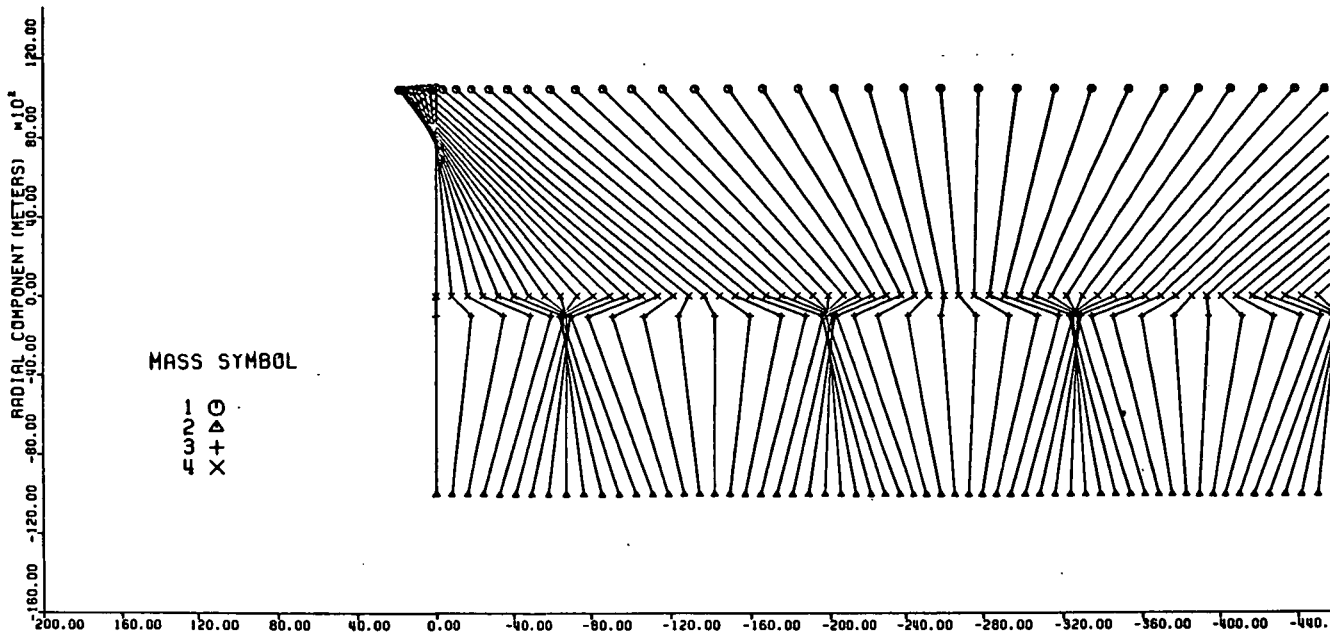


Figure 2.5.2za - Expanded Scale, Front-View Plotted Every 40 Sec for 7200 Sec. Longitudinal + In-Plane Librational/Lateral Dampers On.

dampers upon the in-plane dynamics is evident from the figures.

2.6 Concluding Remarks

The newly developed computer code for 3-dimensional, n-mass tethered systems has been utilized for simulating the free dynamics of a 4-mass tethered system for micro-g/variable-g applications. A new predictor-corrector integrator has been used for the numerical integration of the model. This integrator is up to 40% faster than the older IV-order Runge-Kutta with comparable accuracy. Simulation runs have been performed to show the contributions of the various vibrational modes (librational, longitudinal and lateral) to the dynamics of the system and to the acceleration levels on board the Space Station and the variable-g laboratory. The addition of longitudinal dampers, tuned to the longitudinal vibrational modes, provides an effective damping of the longitudinal oscillatory modes. More sophisticated damping algorithms have also been devised for damping the in-plane librational and lateral oscillations of the system.

3.0 PROBLEMS ENCOUNTERED DURING REPORTING PERIOD

None.

4.0 ACTIVITY PLANNED FOR THE NEXT REPORTING PERIOD

Further investigation and simulation efforts will be carried out on the damping of the out-of-plane oscillatory modes. The modeling of external perturbations will be initiated with the final target of a reliable, accurate model of the J_2 perturbations, atmospheric drag and solar illumination that cause tether expansions and contractions.